Checkpoint inhibition of origin firing prevents DNA topological stress

Esther C. Morafraile[1]*, Christine Hänni[1]*, George Allen[1], Theresa Zeisner[1], Caroline Clarke[1], Mark C. Johnson[1], Miguel M. Santos[1], Lauren Carroll[1], Nicola E. Minchell[3], Jonathan Baxter[3], Peter Banks[2], Dave Lydall[2], Philip Zegerman[1#]

[1] Wellcome Trust/Cancer Research UK Gurdon Institute and Department of Biochemistry, The Henry Wellcome Building of Cancer and Developmental Biology, University of Cambridge CB2 1QN, UK

[2] Institute for Cell and Molecular Biosciences, The Medical School Newcastle University, Newcastle upon Tyne NE2 4HH, UK.

[3] Genome Damage and Stability Centre, Science Park Road, University of Sussex, Falmer, Brighton, East Sussex BN1 9RQ, UK.

* Joint first authorship

[#] Corresponding author and Lead Contact. e-mail: p.zegerman@gurdon.cam.ac.uk

Abstract

A universal feature of DNA damage and replication stress in eukaryotes is the activation of a checkpoint-kinase response. In S-phase, the checkpoint inhibits replication initiation, yet the function of this global block to origin firing remains unknown. To establish the physiological roles of this arm of the checkpoint, we analysed separation of function mutants in the budding yeast *Saccharomyces cerevisiae* that allow global origin firing upon replication stress, despite an otherwise normal checkpoint response. Using genetic screens we show that lack of the checkpoint-block to origin firing results in a dependence on pathways required for the resolution of topological problems. Failure to inhibit replication initiation indeed causes increased DNA catenation, resulting in DNA damage and chromosome loss. We further show that such topological stress is not only a consequence of a failed checkpoint response, but also occurs in an unperturbed S-phase when too many origins fire simultaneously. Together we reveal that the role of limiting the number of replication initiation events is to prevent DNA topological problems, which may be relevant for the treatment of cancer with both topoisomerase and checkpoint inhibitors.

Introduction

To ensure the timely and complete duplication of the genome, eukaryotic chromosomes are replicated from multiple origins. As a result, eukaryotic replication must be strictly regulated so that no origin fires more than once per S-phase. This is achieved by close linkage between replication initiation and cell cycle control (Bell and Labib 2016). The first step in replication (pre-replicative complex assembly or 'licensing') involves the loading of inactive double hexamers of the Mcm2-7 helicase at origins in G1 phase. Initiation at these origins can only occur in S-phase due to the activation of the S-phase CDK (S-CDK) and Dbf4-dependent (DDK) kinases. DDK directly phosphorylates Mcm2-7 double hexamers, while CDK phosphorylates two essential initiation factors Sld3 and Sld2. Together, DDK and CDK are required for the assembly of the active replicative helicase and for the recruitment of additional proteins to form the multi-subunit replication machinery, called the replisome.

Although S-CDK and DDK both accumulate at the G1-S transition, origins do not all fire simultaneously, but instead fire throughout S-phase (Rhind and Gilbert 2013). The timing of firing of an origin is stereotypical, with some origins more likely to fire early in S-phase, some in late S-phase, while others do not fire at all in a normal S-phase, so-called dormant origins (McIntosh and Blow 2012). Origin firing time is affected by several factors, including chromatin environment and subsequent accessibility to limiting replication initiation factors, which include CDK targets Sld2 and Sld3, as well as the DDK subunit Dbf4 (Mantiero et al. 2011; Tanaka et al. 2011). A temporal order of origin firing, together with dormant origins, likely acts as a back up mechanism to ensure complete genome duplication even if irreparable damage occurs at one or more replication forks (McIntosh and Blow 2012).

Replication stress, for example caused by DNA lesions, conflicts between DNA and RNA polymerase or low levels of deoxynucleotide triphosphates (dNTPs), is an early

event during tumourigenesis (Kotsantis et al. 2018). Such stress leads to stalling of the replisome and activation of the checkpoint kinase ATR/Mec1, which causes the subsequent activation of the effector kinase Chk1 in humans or Rad53 in yeast (Giannattasio and Branzei 2017). This response to replication stress is called the S-phase, intra-S-phase or DNA replication checkpoint (Pardo et al. 2017).

The S-phase checkpoint results in a range of responses including the up-regulation of dNTPs, DNA repair and fork stabilisation, which enables forks to resume replication after stalling (Giannattasio and Branzei 2017). In addition, it was observed over 40 years ago that DNA damage results in the inhibition of replication initiation (Painter 1977), which is checkpoint-dependent (Painter and Young 1980). Although the firing of local dormant origins allows stalled replication forks to be rescued, the checkpoint induces a global inhibition of replication initiation resulting in the overall slowing of DNA synthesis in response to damage (Painter 1977; Paulovich and Hartwell 1995; McIntosh and Blow 2012). The function of this global inhibition of origin firing has remained unclear.

The mechanism of inhibition of origin firing by the checkpoint has been established in budding yeast (Lopez-Mosqueda et al. 2010; Zegerman and Diffley 2010). In response to DNA damage or fork stalling agents, the checkpoint kinase Rad53 phosphorylates and inhibits two replication initiation factors, Dbf4 and Sld3. These two substrates are the minimum targets for the checkpoint-dependent block to origin firing, because mutation of the Rad53-phosphorylated residues in Dbf4 and Sld3 allows replication initiation even when Rad53 is fully active (Lopez-Mosqueda et al. 2010; Zegerman and Diffley 2010). Although it is not clear how Rad53 inhibits Dbf4, phosphorylation of Sld3 by Rad53 prevents its interactions with other replication factors including Dpb11 and Cdc45 (Lopez-Mosqueda et al. 2010; Zegerman and Diffley 2010). The checkpoint-inhibition of origin firing is conserved across eukaryotes and there are significant similarities in the mechanism of this control in

metazoa, including the checkpoint inhibition of the Sld3 orthologue Treslin (Guo et al. 2015) and inhibition of DDK (Costanzo et al. 2003).

Here we take advantage of the separation of function alleles of *SLD3* and *DBF4* that cannot be inhibited by Rad53 (Zegerman and Diffley 2010) to analyse the role of the global inhibition of origin firing after replication stress in the budding yeast *Saccharomyces cerevisiae*. We show that a critical consequence of loss of the checkpoint block to initiation is the excessive DNA topological stress generated by large numbers of replication forks, resulting in DNA damage and chromosome loss. This study provides the first analysis of the role of this checkpoint response in isolation, which has implications for why most cells utilise only a fraction of their origins in a normal S-phase.

Results

The replication checkpoint inhibits origin firing genome-wide

Previously we generated alleles of *SLD3* and *DBF4* in budding yeast that cannot be phosphorylated by the checkpoint kinase Rad53 (Zegerman and Diffley 2010). These alleles contain serine/threonine to alanine mutations at thirty-eight sites in Sld3 and four sites in Dbf4 and are hereafter referred to as *sld3-A* and *dbf4-A*. These alleles are effective separation of function mutants because they are fully competent for their essential functions in replication initiation, yet they prevent checkpoint-inhibition of origin firing while checkpoint activation and other functions of this pathway remain unaffected (Zegerman and Diffley 2010, Figure 1B and Supplemental Figure 1A).

To demonstrate the importance of checkpoint-inhibition of origin firing genome-wide, we analysed the replication dynamics of the *sld3-A dbf4-A* strain during replication stress by high-throughput sequencing. Replication profiles were obtained by comparing the DNA content of cells in G1 phase (arrested with the mating

pheromone alpha factor), with those arrested in hydroxyurea (HU) after release from G1. A representative chromosome (Chr XI) from this analysis shows that wild type cells (black line - Figure 1A) initiate replication at early firing origins, but not at late firing origins, as expected due to the activation of the checkpoint (Figure 1B). Importantly in the *sld3-A dbf4-A* mutant strain (blue line - Figure 1A), not only did early origins fire efficiently, e.g ARS1114.5 (red arrow, Figure 1A), so did almost all other annotated origins (e.g green arrows, Figure 1A). Indeed, unannotated origins (see Siow et al. 2012) also fire in the *sld3-A dbf4-A* strain (* Figure 1A), including XI-236 and proARS1110 and proARS1111, consistent with a global effect of the checkpoint on origin firing. Early origins, such as ARS1114.5 (red arrow, Figure 1A), appear to fire even more efficiently in the *sld3-A dbf4-A* strain, likely because the timing of origin firing (T_{rep}) is an average and in some wild type cells this origin is inhibited by the checkpoint. Despite this, the increase in origin firing in the *sld3-A dbf4-A* strain was greatest at late firing origins (Figure 1A and Supplemental Figure 1C), as expected (Zegerman and Diffley 2010).

Genome-wide analysis showed that over 4 times more origins fired in the *sld3-A dbf4-A* strain in HU (Figure 1C), resulting in a greatly reduced inter-origin distance (Figure 1D). The *sld3-A dbf4-A* strain also displays greater Rad53 activation than a wild type strain (Figure 1B and Zegerman and Diffley 2010). Since Rad53 activation is proportional to the number of stalled forks (Tercero et al. 2003), this increased Rad53 activation is likely due to the greater number of forks in the *sld3-A dbf4-A* strain in HU (Figure 1A). In addition, the peaks of replication in the *sld3-A dbf4-A* strain were narrower on average than in a wild type strain (Supplemental Figure 1D), suggesting that although more origins fire in this strain in HU, forks travel less far. This is consistent with previous studies showing that increased origin firing results in reduced fork progression, which in HU is likely due to the limiting pools of dNTPs (Poli et al. 2012; Zhong et al. 2013).

We have previously shown that the *sld3-A dbf4-A* strain has a fast S-phase in the presence of the DNA alkylating agent MMS (Zegerman and Diffley 2010). By performing a similar analysis as in HU, we now show that this fast S-phase in high doses of MMS is indeed due to much greater degree of origin firing in the *sld3-A dbf4-A* strain at 90 minutes (Figure 1E), resulting in near completion of S-phase by 180 mins (Figure 1F and Supplemental Figure 1E). Together, these analyses show that the *sld3-A dbf4-A* alleles are excellent tools to analyse specifically the global inhibition of origin firing by the checkpoint.

Checkpoint inhibition of origin firing prevents the accumulation of DNA damage markers

As the failure of the checkpoint-inhibition of origin firing led to a dramatic increase in replication initiation (Figure 1), we wondered whether this might result in genome instability. To address this we analysed the appearance of markers of DNA damage in the *sld3-A dbf4-A* strain. Checkpoint kinase-mediated phosphorylation of H2A at serine 129 resulting in γH2A (equivalent to metazoan γ-H2AX) is an early response to DNA damage and fork stalling (Szilard et al. 2010; Allen et al. 2011). Analysis of γH2A by western blot revealed that the *sld3-A dbf4-A* mutant strain has higher levels of γH2A than wild type in both HU and MMS, indicative of DNA damage (Figure 2A and Supplemental Figure 2A).

To further detect DNA damage accumulation we analysed the formation Rad52-foci. Rad52 is essential for double strand break (DSB) repair through homologous recombination (HR) and forms foci at DSBs, but also forms foci in response to fork stalling (Lisby et al. 2001; Lisby et al. 2004; Allen et al. 2011). While we observed very little Rad52 foci formation in wild type cells, there was a dramatic increase in Rad52 foci in the *sld3-A dbf4-A* strain in the presence of both HU and MMS (Figure 2B and 2C), consistent with a previous study (Lopez-Mosqueda et al. 2010). These

Rad52 foci were specific to replication stress in S-phase and were not suppressed by inhibiting mitosis or by increasing nucleotide concentrations (Supplemental Figure 2B-D). Although γH2A and Rad52-foci occur at DSBs, the timing of accumulation of Rad52-foci in HU was coincident with S-phase progression (Supplemental Figure 2E). This is consistent with previous reports showing that Rad52 foci can form due to replication stress independently of DSBs (Lisby et al. 2004; Szilard et al. 2010; Allen et al. 2011).

Checkpoint defective strains, such as *RAD53* null mutants, have been previously shown to accumulate Rad52 foci after fork stalling (Lisby et al. 2004). Significantly, a comparison between *sld3-A dbf4-A* and *rad53*Δ cells shows that the failure to inhibit origin firing accounts for the majority of Rad52 foci in this checkpoint mutant (Figure 2D). Significantly the *sld3-A dbf4-A* and *rad53*Δ alleles are epistatic for the formation of Rad52-foci (Figure 2D), consistent with these mutants generating Rad52-foci by the same mechanism. From these data we conclude that the checkpoint-dependent inhibition of origin firing is an important pathway to prevent DNA damage marker accumulation in S-phase.

Checkpoint inhibition of origin firing prevents DNA damage globally, but in particular at convergently transcribed genes

To determine whether the increase in γH2A and Rad52-foci after loss of the checkpoint inhibition of origin firing (Figure 2) is due to genome instability at specific loci, we decided to map the location of these DNA damage markers. γ-H2A ChIP shows that in the wild type strain, γ-H2A accumulated around early origins, but not late origins (Figure 3A and Supplemental Figure 3A). This likely reflects the fact that γ-H2A only accumulates at replicating loci. In accordance with this, the *sld3-A dbf4-A* strain, which allows initiation at early and late origins in HU (Figure 1A), accumulated γ-H2A around both early and late firing origins (Figure 3A and Supplemental Figure

3A). This γ-H2A ChIP was specific for the modified form of H2A, as no enrichment was observed in strains containing the *h2a-S129A* mutation, which lacks the phosphorylated serine (red lines - Figure 3A) nor in strains lacking the kinases that phosphorylate H2A-S129 (*mec1*Δ *tel1*Δ, blue lines - Figure 3A).

To determine whether γ-H2A preferentially accumulated at specific loci, we analysed the location of the γ-H2A peaks. Showing chromosome XI as a representative snapshot of the genome, the peaks of γ-H2A were distributed throughout the chromosome for both the wild type and *sld3-A dbf4-A* strains (Figure 3B). For *sld3-A dbf4-A* there are some unique peaks compared to wild type at normally late firing origins (e.g orange arrow - Figure 3B), consistent with *sld3-A dbf4-A* permitting replication initiation at those origins (see Supplemental Figure 3B for overlay between γ-H2A and replication). Despite this, there are some sites that replicate efficiently in the *sld3-A dbf4-A* strain but accumulate only a small amount of γ-H2A (such as ARS1107, black arrow - Figure 3B) and conversely there are other origins where a small increase in replication leads to a greater γ-H2A signal (e.g ARS1123, pink arrow - Figure 3B). Such differences are suggestive of some genomic bias in γ-H2A accumulation.

To identify loci that are susceptible to damage and to account for differences in replication between the strains we normalised the γ-H2A signal at each genomic locus to the amount of replication at that location. From this analysis we did not observe a correlation between γ-H2A and tRNA genes, telomeres, Ty elements, LTRs and centromeres (data not shown). We did however observe a significant enrichment of γ-H2A in the *sld3-A dbf4-A* strain at gene pairs where the direction of transcription converges upon the direction of replication (hereafter called convergent gene pairs, Figure 3C). This correlation was specific to convergent gene pairs, not co-directional or divergent gene pairs (Figure 3D). Interestingly, the enrichment of γ-

H2A at convergent gene pairs increased with T_{rep} (Figure 3C). This correlation is not due to a bias in the distribution of convergent gene pairs around late origins (Supplemental Figure 3C).

To confirm the γ-H2A DNA damage mapping results, we also performed ChIP for Rad52-GFP from cells treated with MMS for 90 and 180 minutes (Supplemental Figure 4). This anti-GFP ChIP showed great similarity with the γ-H2A ChIP in that Rad52 was distributed throughout the genome, with enrichment at convergent gene pairs, not at non-convergent gene pairs (Supplemental Figure 4). Together these ChIP analyses show that in the absence of checkpoint inhibition of origin firing, DNA damage markers appear throughout the genome with some enrichment at convergently transcribed gene pairs.

Genetic screens identify pathways that are important in the absence of checkpoint-inhibition of origin firing

The mapping of DNA damage markers (Figure 3) suggested that the failure to inhibit origin firing in the *sld3-A dbf4-A* strain causes DNA damage throughout the genome. To identify in an unbiased way the potential cause of such DNA damage, we conducted genetic screens between the *sld3-A dbf4-A* alleles and the entire yeast gene knockout collection (Addinall et al. 2011; Holstein et al. 2018). Many essential genes were also represented in this screen by including the DAmP (Decreased Abundance by mRNA Perturbation) allele collection, whereby mRNAs are destabilised through perturbation of the 3'UTR (Breslow et al. 2008). For this screen we used a quantitative fitness analysis (QFA) approach, which is a high-throughput growth analysis method in solid medium (Addinall et al. 2011; Holstein et al. 2018).

The fitness of every gene deletion (your favourite gene deletion, *yfg*Δ) and *yfg*Δ *sld3-A dbf4-A* was measured in quadruplicate in HU (Figure 4A and Supplemental Table 1). Figure 4A highlights the *yfg*Δ *sld3-A dbf4-A* strains that grew significantly better

241 than the equivalent *yfg*Δ alone (red dots, Figure 4A) and these *yfg*Δ are hereafter
242 classified as *sld3-A dbf4-A* suppressors. Conversely the *yfg*Δ mutations that
243 conferred worse growth with *sld3-A dbf4-A* are classified as enhancers (green dots,
244 Figure 4A). Gene ontology (GO) analysis of the enhancers in HU revealed an
245 enrichment for genes involved in DNA/RNA metabolism and chromosome fidelity
246 (Supplemental Figure 5A and Supplemental Table 2). We validated this screen by
247 generating null alleles of seventeen of the enhancer hits in a different yeast strain
248 (W303) and confirming the growth defect with *sld3-A dbf4-A* (data not shown).
249 Analysis of the *sld3-A dbf4-A* enhancers relative to known protein complexes (Pu et
250 al. 2009) identified several complexes as significant hits (Figure 4A and 4B),
251 including the THO complex, which is required for the resolution of R-loops, the
252 Holliday junction resolvase Mus81/Mms4 and the CTM (Csm3/Tof1/Mrc1) complex,
253 which maintains fork stability (Schalbetter et al. 2015; Brambati et al. 2018; Duch et
254 al. 2018).

255 To further focus on the pathways that are important in the absence of checkpoint-
256 inhibition of origin firing, we also performed the genetic screen using another
257 genotoxic agent, phleomycin. In order to compare directly between screens a genetic
258 interaction strength (GIS) score (Addinall et al. 2011) was used to define the relative
259 growth of each *yfg*Δ *sld3-A dbf4-A* strain compared to the modelled average fitness
260 of the population of strains (black line, Figure 4A for HU). A negative GIS for a *yfg*Δ,
261 indicates worse growth than expected when combined with *sld3-A dbf4-A*
262 (enhancers), while a positive GIS indicates better growth of *yfg*Δ *sld3-A dbf4-A* than
263 expected (suppressors). Plotting the GIS scores for the HU hits against the
264 phleomycin hits highlights genes identified by both screens (Figure 4C and
265 Supplemental Table 3). The HU and phleomycin screens showed a high degree of
266 overlap between the enhancers and suppressors (Supplemental Figure 5B). As in
267 Figure 4B, we identified protein complexes that were enriched as enhancers or

suppressors in both screens (Figure 4D and Supplemental Figure 5C). Notable enhancers (Figure 4C and 4D) include the type I topoisomerase Top1 and the CTM complex, as well as genes required for chromosome transmission fidelity, such as spindle assembly checkpoint (Bub1, Bub3), kinetochore (Mcm16, Mcm22) and cohesin loading factors (Ctf18 complex). The elongator complex was also identified in other QFA screens (Addinall et al. 2011), suggesting that it may be a false positive.

A similar analysis of the suppressors revealed genes required for mitochondrial function as well as the OCA tyrosine phosphatase complex (Figure 4C and Supplemental Figure 5C). Both mitochondrial mutants and the OCA complex were identified as suppressors of uncapped telomeres (Addinall et al. 2008), suggesting that they are common false positives or that they suppress multiple pathways of genome instability. Together, these genome-wide genetic screens identified key chromosomal maintenance pathways that are necessary for survival in the absence of checkpoint inhibition of origin firing during replication stress.

A longstanding hypothesis for the role of the inhibition of origin firing after DNA damage is to create a time window for repair to occur (Painter and Young 1980; Paulovich and Hartwell 1995). From this, we would expect mutations in repair pathways to be significant enhancer hits from these screens, but this was not the case (Supplemental Table 1 and 3). To further examine this hypothesis we made mutations in eight different repair pathways and tested their genetic interactions with *sld3-A dbf4-A* in a range of different DNA damaging agents (Supplemental Figure 5D). Consistent with the formation of Rad52 foci in the *sld3-A dbf4-A* strain, we did observe synthetic sickness between *sld3-A dbf4-A* and null mutations in *RAD52* and another HR factor *RAD50*, but not with any other DNA repair mutation (Supplemental Figure 5D). This suggests that facilitating repair of exogenous damage is not a major physiological role of the checkpoint inhibition of origin firing (see Discussion).

Checkpoint inhibition of origin firing prevents excess catenation and chromosome loss

DNA replication generates supercoiling ahead of the fork, which is relieved by topoisomerases. This supercoiling can also be converted into catenanes behind the fork (precatenanes) by fork rotation, which is likely to be particularly important when topoisomerase action is restricted for example during replication termination (Peter et al. 1998; Schalbetter et al. 2015). The unbiased genetic screens showed that Top1, which removes supercoiling, and Csm3, which restrains fork rotation are important for viability in the *sld3-A dbf4-A* strain (Figure 4). From these genetic interactions, together with the dramatic increase in fork number in the *sld3-A dbf4-A* strain (Figure 1) we hypothesised that there might be an increase in topological problems when the checkpoint fails to limit origin firing.

To test this we used an *in vivo* plasmid-based assay that detects the degree of supercoiling and fork rotation during replication through the accumulation of catenanes (CatA, Schalbetter et al. 2015). This assay is performed in the absence of Top2 (here we use the conditional mutant *top2-4*), to ensure that catenanes are preserved after replication (Figure 5A). 2D gel analysis of plasmids replicated in MMS showed that there is little difference between the wild type and *sld3-A dbf4-A* strain in the catenation of a plasmid where the replication fork and the transcription unit are co-directional (plasmid 1184, Figure 5B and 5D). Interestingly however, when we flipped the orientation of the marker gene, so that transcription and replication are convergent on the plasmid, we observed an increase in the median number of catenanes specifically in the *sld3-A dbf4-A* strain (plasmid 1185, Figure 5A, 5C and 5D). These data show that checkpoint-inhibition of origin firing prevents the accumulation of topological problems during S-phase at sites of convergent transcription and replication.

Failure to remove catenanes results in nondisjunction in mitosis (Holm et al. 1989) and we wondered whether the excessive topological constraints resulting from failure of the checkpoint to inhibit origin firing might also result in chromosomal abnormalities. Failure to inhibit origin firing indeed resulted in a 2-fold increased loss-rate of a plasmid in HU (plasmid 809, Figure 5E), indicative of increased chromosome loss. This plasmid loss phenotype was not due to differences in origin firing as this plasmid initiates replication early and fires equally in both the wild type and *sld3-A dbf4-A* strains, as expected (Supplemental Figure 6A).

As we observed increased topological problems due to convergence between replication and transcription (Figure 5A-D), we wondered whether such conflicts might render a plasmid more susceptible to loss in the *sld3-A dbf4-A* strain. To test this we added an additional ADE2 marker to the plasmid, transcribed either co-directionally with replication (plasmid 863) or transcribed convergently to the replication fork (plasmid 862, Figure 5E). Although the co-directional plasmid was lost as frequently as the parental plasmid 809, convergent transcription indeed resulted in greater plasmid loss in the *sld3-A dbf4-A* strain in HU (Figure 5E). The enhanced plasmid loss due to convergent transcription was unlikely due to inhibition of the plasmid origin because we did not observe this effect in the absence of HU (Supplemental Figure 6B).

To further detect chromosomal abnormalities, we analysed the transmission of yeast chromosomes during mitosis. Using myosin-GFP to label the contractile ring during cytokinesis and histone H2B-mCherry to visualise chromosomes, we measured the persistence of mitotic chromosomes in the bud neck, which is indicative of incomplete replication and failed segregation (Amaral et al. 2016). Significantly, we observed an increase in chromosomal DNA persisting in the bud neck during ring contraction in the *sld3-A dbf4-A* strain (Figure 5F), suggestive of delayed replication termination or decatenation in the absence of checkpoint inhibition of origin firing.

Together these analyses show that under replication stress the failure to inhibit origin firing causes topological problems to accumulate in S-phase (Figure 5A-D) and results in defects in chromosome segregation (Figure 5E-F), both of which are exacerbated at sites of convergent transcription-replication (Figure 5B-E).

Topological defects exacerbate the genetic interactions and underlie the accumulation of DNA damage in the *sld3-A dbf4-A* strain

Many of the pathways identified in the genetic screens (Figure 4) are either required to resolve DNA topological problems (Top1 and Csm3/Tof1) or are required to suppress the genome instability that arises from topological problems such as R-loops (e.g THO complex, Tuduri et al. 2009; El Hage et al. 2010) or terminal replication structures (Mus81/Mms4, Regairaz et al. 2011). Therefore, we hypothesised that if the topological issues caused by increased origin firing (Figure 5) are physiologically important then reducing topoisomerase activity together with *sld3-A dbf4-A* should enhance the genetic interactions with other chromosome maintenance pathways.

Combining *sld3-A dbf4-A* with a null mutation in the type I topoisomerase (*top1*Δ) indeed led to a much greater synthetic sickness with null mutations in genes required to prevent fork rotation (Tof1, Csm3, Figure 6A and Supplemental Figure 6C). This genetic interaction was not specific to loss of Top1, as a hypomorphic mutation in Top2 also caused synthetic sickness with *sld3-A dbf4-A* and *tof1*Δ (Supplemental Figure 6D). These genetic interactions suggest that the topological problems generated by global origin firing (Figure 5A-D) become overwhelming when pathways that resolve supercoiling or catenation are compromised.

R-loops and chromosome non-disjunction are consequences of topological problems (Holm et al. 1989). Combining *sld3-A dbf4-A top1*Δ with a mutant defective in R-loop resolution (*thp2*Δ, Figure 6B) as well as chromosome segregation mutants *bub3*Δ

and *ctf18*Δ (Supplemental Figure 6F and Figure 6C) indeed led to a synergistic synthetic sickness. Relief of topological problems is also particularly important at replication termination, when converging forks meet (Branzei and Foiani 2010). As a result, we observed a robust synthetic sickness between *sld3-A dbf4-A top1*Δ and null mutations in the Mus81/Mms4 complex (Figure 6D and Supplemental Figure 6G) as well as the Sgs1 helicase (Figure 6E), which are important for resolving persistent and terminal replication intermediates (Regairaz et al. 2011; Cejka et al. 2012). In line with this genetic data, null mutations in Top1 and Mus81 combined with *sld3-A dbf4-A* caused increased levels of nuclear fragmentation after mitosis (Figure 6F). Such fragmentation is indicative of failures in replication completion/chromosome segregation in these mutants. Together these data show that defects in topoisomerases greatly enhance the genetic interactions of *sld3-A dbf4-A* identified in Figure 4, suggesting that topological problems are a major consequence of loss of checkpoint control of origin firing.

DNA damage markers, such as Rad52 foci, accumulate genome-wide in the *sld3-A dbf4-A* strain, with some enrichment at convergently transcribed gene pairs (Figure 3 and Supplementary Figure 4). If these DNA damage markers occur in response to topological problems then we would expect them to increase when decatenation/relaxation activities are compromised and conversely we might expect them to be suppressed if topoisomerases are over-expressed. Indeed we observed an increase in Rad52 foci in the *sld3-A dbf4-A* strains that also lack Tof1 (Supplemental Figure 7A) and Top1 (Supplemental Figure 7B). Unfortunately efforts to suppress this DNA damage by over-expression of either Top2 or Top1 were hampered by the fact that over-expression of either protein causes genome instability and death in yeast (Nitiss et al. 2001; Sen et al. 2016). Despite this, we found that an N-terminally tagged Top2 was highly unstable, allowing it to be temporarily over-expressed in S-phase (Supplemental Figure 7C). Importantly, expression of this

unstable form of Top2 was sufficient to partially suppress the appearance of Rad52 foci in the *sld3-A dbf4-A* strain (Figure 6G). We also observed a partial suppression of Rad52 foci by over-expressing Csm3 and Tof1, which prevent precatenane formation (Figure 6H and Supplemental Figure 7D). Together, the enhanced synthetic lethality and chromosomal defects by combining *sld3-A dbf4-A* and topoisomerase mutants (Figure 6A-F), together with the partial suppression of DNA damage by over-expression of Top2 or Csm3/Tof1 (Figure 6G-H) suggest that the accumulation of topological problems is a significant consequence of loss of checkpoint inhibition of origin firing.

High rates of replication initiation in a normal S-phase causes similar phenotypes to failure of checkpoint inhibition of origin firing

Thus far we have used the separation of function mutants, *sld3-A dbf4-A*, to show that increased replication initiation after replication stress leads to topological problems, subsequent DNA damage and genome instability (Figure 5 and 6). It is unclear from these experiments what the importance of replication stress is in creating these problems. Perhaps replication stress generates an increased dependence on topoisomerase or fork rotation activities, possibly due to DNA repair. Alternatively it may be that the excessive number of replication forks is sufficient to cause topological problems and subsequent DNA damage. To distinguish between these possibilities we utilised a yeast strain that can conditionally increase the number of replication initiation events in a normal S-phase (Mantiero et al. 2011). Over-expression of limiting replication factors (Sld3, Sld2, Dpb11, Dbf4, Cdc45 and Sld7, abbreviated to SSDDCS) causes many origins to fire earlier than they would in a normal cell cycle, resulting in a faster S-phase (Mantiero et al. 2011). Importantly we show that over-expression of limiting replication factors in a single cell cycle, in the complete absence of exogenous DNA damage or fork stalling agents, also leads to the accumulation of both Rad52 foci and γH2A in S-phase (Figure 7A and 7B).

Increased rates of replication in a normal S-phase leads to the depletion of dNTPs and Rad53 activation, which can be suppressed by the deletion of the RNR inhibitor *SML1* (Mantiero et al. 2011). Deletion of *SML1* did not affect the accumulation of Rad52-foci, nor γH2A, suggesting that this is not a consequence of dNTP depletion or Rad53 activation (Figure 7A and 7B). We also observed that the SSDDCS strain exhibits synthetic sickness with a hypomorphic mutant of Top2 (Figure 7C), suggesting that excessive origin firing in a normal S-phase indeed leads to greater dependence on topoisomerases. Importantly, we observed that high rates of initiation in a normal S-phase also resulted in increased catenation of a replicated plasmid *in vivo* (Figure 7D and 7E). These data show that the phenotypes associated with the *sld3-A dbf4-A* strain undergoing replication stress, such as DNA damage (Figure 2), genetic interactions with topoisomerases (Figure 4 and 6) and accumulation of catenanes on a mini-chromosome *in vivo* (Figure 5A-D) also occur when the levels of replication initiation are increased in an otherwise normal S-phase.

If it is the excess of normal forks, rather than stalled forks, that causes topological problems, then we hypothesised that DNA damage should occur in the *sld3-A dbf4-A* strain even after HU treatment, when fork stalling has abated. To test this we first arrested yeast cells in 200mM HU for 90 minutes to allow almost all origins to fire and stall in the *sld3-A dbf4-A* strain (Figure 1A), and then we released the cells into fresh medium lacking HU to observe when Rad52-foci accumulate. After 90 minutes in HU when most forks are stalled and Rad53 is active (Supplementary Figure 7F), we observed very low amounts of Rad52 foci (Figure 7F). This suggests that fork stalling by itself is not the cause of Rad52 foci in the *sld3-A dbf4-A* strain. Importantly when we released these cells in the absence of HU, allowing forks to progress and terminate, we observed a dramatic increase in Rad52-foci, coincident with S-phase progression (Figure 7F and 7G). The *sld3-A dbf4-A* strain exhibited delayed progression through mitosis (Figure 7G), consistent with defects in the completion of

454 replication in this strain in HU (Figure 5F). Together these experiments suggest that
455 excessive replication initiation, followed by high levels of normal fork progression is
456 an important driver of topological stress and the accumulation of DNA damage
457 markers.

Discussion

Role of checkpoint inhibition of origin firing

Over 40 years ago it was first established that eukaryotes inhibit replication initiation in the face of DNA damage (Painter 1977). By using specific separation of function mutants, our data suggests that the checkpoint limits the total number of simultaneous forks in order to maintain the balance between fork progression and topoisomerase/fork rotation activities (Figure 7H). We provide direct evidence that under conditions when excessive origins fire, both in the presence of DNA damage and in a normal S-phase, topological linkages accumulate *in vivo* (Figure 5A-D and Figure 7D-E). Failures to resolve supercoiling and catenation in a timely manner is a likely source for the DNA damage and chromosome segregation defects that occur when excessive origins fire and this DNA damage can indeed be suppressed by overexpression of topoisomerase (Figure 6). Since transcription also generates positive supercoiling, failure to resolve topological problems may explain why convergent replication-transcription units are prone to accumulate excess catenation (Figure 5A-D) and why convergently transcribed gene pairs accumulate DNA damage in the *sld3-A dbf4-A* strain (Figure 3C). The overwhelming of topoisomerase activities also explains why topological problems can occur in trans on episomal plasmids with only a single origin (Figure 5A-D and Figure 7D-E). As Top1 is known to bind to the replisome, possibly through interactions with Tof1 (Bell and Labib 2016), large numbers of replication forks progressing simultaneously might result in depletion of topoisomerase activities, affecting forks in trans. Consistent with our model (Figure 7H), DNA damage accumulates during normal fork progression (when topoisomerases are required) not during fork stalling (Figure 7A-G) .

A longstanding hypothesis for the role of the checkpoint in delaying S-phase progression is that blocking origin firing allows more time for DNA repair to occur

(Painter and Young 1980; Paulovich et al. 1997). Our data suggest that this is not a primary role for the checkpoint inhibition of firing. First of all, the whole genome and targeted screens did not identify genetic interactions between *sld3-A dbf4-A* and many repair pathways (Supplemental Table 1 and 3 and Supplemental Figure 5D). Furthermore a strain that fires multiple origins simultaneously, even in the absence of any exogenous genotoxins, also causes DNA damage and the accumulation of topological problems (Figure 7A-E). In addition, fork stalling is not the driver of Rad52-foci accumulation in the *sld3-A dbf4-A* strain (Figure 7F-G). Rather than needing time for repair, stalled forks are actually rescued by forks emanating from neighbouring dormant origins even in checkpoint proficient cells (McIntosh and Blow 2012). Our data suggests it is the global level of origin firing which is important to prevent topological constraints during S-phase, irrespective of exogenous DNA damage (Figure 7H).

While we show that topological defects are important to generate Rad52-foci (Figure 6G-H), the function of Rad52 in the absence of checkpoint inhibition of origin firing is not clear. We cannot rule out that DSBs do form at some point due to excess origin firing, but we note that HR proteins resolve replication fork intermediates in the absence of DSBs (Kolinjivadi et al. 2017; Ait Saada et al. 2018). Indeed, a significant consequence of topological defects is fork reversal, whereby positive supercoiling ahead of the replisome drives nascent DNA at the fork to regress and anneal to generate a four-way junction (Postow et al. 2001; Neelsen and Lopes 2015). Interestingly a recent study has shown a role for Rad52 in protection of reversed forks from degradation (Malacaria et al. 2019). It is also notable that Rad52-foci and γH2A occur in response to RNA-DNA hybrids (Costantino and Koshland 2018; Garcia-Rubio et al. 2018). The genetic interactions with pathways required for R-loop resolution and the accumulation of DNA damage markers at convergent genes (Figure 4A and 3C), suggests that R-loops may also be a consequence of excessive

origin firing, possibly also as a downstream consequence of topological problems (Figure 7H, Hamperl and Cimprich 2014).

Although we show here that topological stress is a prominent consequence of failure of checkpoint inhibition of origin firing, the synthetic lethality screens also identified other processes that may be affected by this checkpoint pathway (Figure 4). One example is the histone variant H2A.Z (Htz1 in yeast) and its associated remodelling complex Swr1, which were significant hits from both screens (Figure 4D). Swr1/Htz1 have roles in many cellular processes, such as transcription and chromatin maintenance (Morrison and Shen 2009). Despite this, we note that Swr1/Htz1 also have roles in response to replication stress and CTM complex function (Morrison and Shen 2009; Srivatsan et al. 2018), so their genetic interaction with *sld3-A dbf4-A* may still be related to the topological problems described here.

Topological stress as a branch of replication stress

'Replication stress' is a frequently used term that encompasses a wide-range of different genome maintenance events (Kotsantis et al. 2018). By utilising separation of function mutants, here we have isolated a specific form of replication stress caused by too much origin firing (Figure 7H). The identification of topological problems as a branch of replication stress may contribute to our understanding of the locations and mechanisms of genome instability. For example, sites of convergent replication-transcription conflicts have increased genome instability (Hamperl et al. 2017). The topological stress described here may underlie DNA damage at locations or under conditions that affect replication efficiency, transcriptional direction, supercoiling and topoisomerase availability/accessibility.

Eukaryotes license many more origins than are necessary to ensure complete genome replication (McIntosh and Blow 2012). Our data shows that topological stress is generated even in a normal S-phase when too many origins fire (Figure 7C-

E), perhaps explaining why most cells use only a subset of their potential origins. In the early embryonic divisions of many metazoa, such as flies and frogs, S-phase is incredibly short due to very high rates of replication initiation. These early divisions occur in the near absence of transcription, which may be one explanation for how these cells avoid genome instability, but it will be interesting to understand how embryonic cells, but not somatic cells, cope with high rates of topological stress. Furthermore topoisomerase and checkpoint inhibitors are potential combinatorial therapies for the treatment of cancers (Josse et al. 2014; Thomas et al. 2018). This study reveals that unbridled origin firing creates an enhanced dependence on topoisomerase activity, which may provide a new mechanistic rationale for the use of combined checkpoint/topoisomerase inhibition therapies.

548 # Materials and methods

549 ## Strains and Growth Conditions

550 All yeast strains are derived from W303-1a, see Supplemental Table 4. Cell growth,
551 arrests, flow cytometry and yeast protein extracts were as previously described
552 (Zegerman and Diffley 2010).

553 ## Replication Profiles

554 Yeast genomic DNA was extracted using the spheroplast method (*http://fangman-*
555 *brewergeneticswashingtonedu/indexhtml*). Samples were prepared according to the
556 TruSeq Nano sample preparation guide from Illumina. To generate replication timing
557 profiles, the ratio of uniquely mapped reads in the replicating samples to the non-
558 replicating samples was calculated following (Muller et al. 2014) and profiles were
559 smoothed by a Fourier transformation (Muller et al. 2014). A replication peak was
560 defined as a curve point where the S to G1 ratio/Δkb changed from plus to minus and
561 the same sign was kept at more than 3kb from the change point. A peak is therefore
562 defined as a local maximum. The values of T_{rep} were from OriDB (Siow et al. 2012).

563 ## Chromatin Immunoprecipitation-Sequencing (ChIP-Seq)

564 As previously described (Can et al. 2019). Antibodies for IP were Anti-H2A (39945,
565 Actif motif), IgG (AB27478, Abcam) or Anti-γH2A (AB15083, Abcam) or Anti-GFP
566 (3h9, Chromotek).

567 ## Whole genome synthetic lethality screen

568 Synthetic Genetic Array (SGA) was used as described in (Tong and Boone 2006;
569 Holstein et al. 2018) to create two independent strain libraries using a BM3 colony
570 pinning robot (S&P Robotics). The starter strains used were DLY8000 *MAT alpha*
571 *lyp1::HPHMH::NATMX can1delta::STE2pr-Sp_his5 his3Δ leu2Δ ura3Δ met15Δ p*
572 LEU2-sld3-A dbf4-A. and DLY7388 *MAT alpha lyp1::LEU2::HPHMH::NATMX*

573 *can1delta::STE2pr-Sp_his5 his3Δ leu2Δ ura3Δ met15Δ,* as control. The strain
574 libraries used were the yeast knockout (YKO) collection (a kind gift from Charlie
575 Boone) and the DAmP collection (purchased from Open Biosystems now Dharmacon
576 Horizon catalogue number YSC5090). Following SGA we used Quantitative Fitness
577 Analysis (QFA) (Addinall et al. 2008; Addinall et al. 2011; Holstein et al. 2018) to
578 determine the fitness of the strains within the two libraries. Independent 200ul liquid
579 cultures of each strain were grown to saturation using a BM3 colony pinning robot
580 (S&P Robotics), diluted in sterile water and spotted onto the same solid media used
581 in the final SGA selection stage. This media was synthetic defined media
582 (Formedium YNBMSG02) lacking the amino acids arginine, histidine, leucine and
583 lysine with canavanine (50ug/ml Sigma C9758) and thialysine (50ug/ml Sigma
584 A2636) and also containing the antibiotics G418 (200ug/ml Sigma A1720), ClonNat
585 (100ug/ml, Werner BioAgents 5.001.000) and Hygromycin (300ug/ml Sigma H3274)
586 (Holstein et al. 2018). The strains were spotted on the synthetic media which
587 contained no compounds, 2ug/ml Phleomycin or 50mM Hydroxyurea using a
588 Beckman Coulter FX robot and photographed every 4 hours over 5 days. Solid agar
589 plates were photographed on a spImager (S&P Robotics) with an integrated camera.
590 Manual settings of the camera were as follows: 0.25 s; aperture, F10; white balance,
591 3700 K; ISO100; image size, large; image quality, fine; image type, .jpg. Culture
592 density was generated from captured photographs using the Integrated Optical
593 Density measure of cell density provided by the image analysis tool Colonyzer. In
594 order to calculate the fitness, the maximum doubling potential (MDP, population
595 doublings) was multiplied by the maximum doubling rate (MDR, population
596 doublings/day), and the mean value of four replicates was calculated
597 (Tong and Boone 2006; Addinall et al. 2008; Addinall et al. 2011; Holstein et al.
598 2018). The database used for the identification of enriched protein complexes was
599 cyc2008 (Pu et al. 2009).

600 **Microscopy**

601 Samples were plated onto 35mm Glass Bottom plates (MatTek) pre-coated with
602 Concanavalin A (Sigma). After 5mins, cells were imaged on a Deltavision widefield
603 fluorescent microscope (GE Healthcare) using an Olympus 60x objective. Images
604 were acquired, deconvoluted and projected using SoftWoRx (GE Healthcare,
605 Chicago). Analysis of DNA in the bud-neck utilised a plugin for FIJI. At least 200
606 cells were counted for every timepoint.

607 **Western blot**

608 Detection of Rad53 was performed using ab104232 (Abcam, 1:5000), H2A with
609 ab13923 (Abcam, 1:1000) and γH2A (phospho S129) with ab15083 (Abcam, 1:1000).

610 **Plasmid loss**

611 Cultures were pre-grown in selective medium (YPD+hygromycin 500 μg/ml) and then
612 diluted into non-selective medium YPGal + 20mM HU and grown overnight at 30°C.
613 Once the cultures had reached mid-log phase, 100 cells were plate on YPD with or
614 without hygromycin. The rate of plasmid loss per generation was calculated using the
615 formula 100 x (1-RMP $^{1/G}$), where RMP is the ratio of plasmid maintenance (number
616 of colonies on YPD+ hygromycin/number of colonies on YPD) and G is the number of
617 generations during the overnight culture.

618 **Detection of Plasmid Catenation**

619 As described (Schalbetter et al. 2015).

620

Acknowledgments

We thank Gilles Charvin, David Morgan and Steve Jackson for strains, Richard Butler for development of an ImageJ plugin and Alan Leake for assistance with the genetic screens. We thank members of the Zegerman lab for critical reading of the manuscript. Work in the PZ lab was supported by AICR 10-0908, Wellcome Trust 107056/Z/15/Z, Cancer Research UK C15873/A12700 and Gurdon Institute funding (Cancer Research UK C6946/A14492, Wellcome Trust 092096). Part III undergraduate students, LC, TZ and CC were supported by the Department of Biochemistry. MS was funded by the BBSRC BB/M011194/1 and CH by a CRUK Cambridge Centre Non-Clinical Training Award C37096/A13001. JB, NEM and PB, DL were funded by BBSRC BB/S001425/1 and BB/M002314/1 respectively.

Author Contributions

The whole genome synthetic lethality screens were conducted by PB and DL. 2D gel analyses of catenated plasmids were performed by ECM with guidance from NEM and JB. GA and MS performed the bioinformatic analyses. All the experiments were performed and designed by ECM, CH, TZ, CC, LC, MJ and PZ. PZ wrote the paper.

References

Addinall SG, Downey M, Yu M, Zubko MK, Dewar J, Leake A, Hallinan J, Shaw O, James K, Wilkinson DJ et al. 2008. A genomewide suppressor and enhancer analysis of cdc13-1 reveals varied cellular processes influencing telomere capping in Saccharomyces cerevisiae. *Genetics* **180**: 2251-2266.

Addinall SG, Holstein EM, Lawless C, Yu M, Chapman K, Banks AP, Ngo HP, Maringele L, Taschuk M, Young A et al. 2011. Quantitative fitness analysis shows that NMD proteins and many other protein complexes suppress or enhance distinct telomere cap defects. *PLoS genetics* **7**: e1001362.

Ait Saada A, Lambert SAE, Carr AM. 2018. Preserving replication fork integrity and competence via the homologous recombination pathway. *DNA repair* **71**: 135-147.

Allen C, Ashley AK, Hromas R, Nickoloff JA. 2011. More forks on the road to replication stress recovery. *Journal of molecular cell biology* **3**: 4-12.

Amaral N, Vendrell A, Funaya C, Idrissi FZ, Maier M, Kumar A, Neurohr G, Colomina N, Torres-Rosell J, Geli MI et al. 2016. The Aurora-B-dependent NoCut checkpoint prevents damage of anaphase bridges after DNA replication stress. *Nature cell biology* **18**: 516-526.

Bell SP, Labib K. 2016. Chromosome Duplication in Saccharomyces cerevisiae. *Genetics* **203**: 1027-1067.

Brambati A, Zardoni L, Achar YJ, Piccini D, Galanti L, Colosio A, Foiani M, Liberi G. 2018. Dormant origins and fork protection mechanisms rescue sister forks arrested by transcription. *Nucleic acids research* **46**: 1227-1239.

Branzei D, Foiani M. 2010. Maintaining genome stability at the replication fork. *Nature reviews Molecular cell biology* **11**: 208-219.

Breslow DK, Cameron DM, Collins SR, Schuldiner M, Stewart-Ornstein J, Newman HW, Braun S, Madhani HD, Krogan NJ, Weissman JS. 2008. A comprehensive strategy enabling high-resolution functional analysis of the yeast genome. *Nature methods* **5**: 711-718.

Can G, Kauerhof AC, Macak D, Zegerman P. 2019. Helicase Subunit Cdc45 Targets the Checkpoint Kinase Rad53 to Both Replication Initiation and Elongation Complexes after Fork Stalling. *Molecular cell* **73**: 562-573 e563.

Cejka P, Plank JL, Dombrowski CC, Kowalczykowski SC. 2012. Decatenation of DNA by the S. cerevisiae Sgs1-Top3-Rmi1 and RPA complex: a mechanism for disentangling chromosomes. *Molecular cell* **47**: 886-896.

Costantino L, Koshland D. 2018. Genome-wide Map of R-Loop-Induced Damage Reveals How a Subset of R-Loops Contributes to Genomic Instability. *Molecular cell* **71**: 487-497 e483.

Costanzo V, Shechter D, Lupardus PJ, Cimprich KA, Gottesman M, Gautier J. 2003. An ATR- and Cdc7-dependent DNA damage checkpoint that inhibits initiation of DNA replication. *Molecular cell* **11**: 203-213.

Duch A, Canal B, Barroso SI, Garcia-Rubio M, Seisenbacher G, Aguilera A, de Nadal E, Posas F. 2018. Multiple signaling kinases target Mrc1 to prevent genomic instability triggered by transcription-replication conflicts. *Nature communications* **9**: 379.

El Hage A, French SL, Beyer AL, Tollervey D. 2010. Loss of Topoisomerase I leads to R-loop-mediated transcriptional blocks during ribosomal RNA synthesis. *Genes & development* **24**: 1546-1558.

Garcia-Rubio M, Aguilera P, Lafuente-Barquero J, Ruiz JF, Simon MN, Geli V, Rondon AG, Aguilera A. 2018. Yra1-bound RNA-DNA hybrids cause orientation-independent transcription-replication collisions and telomere instability. *Genes & development* **32**: 965-977.

Garcia-Rubio ML, Aguilera A. 2012. Topological constraints impair RNA polymerase II transcription and causes instability of plasmid-borne convergent genes. *Nucleic acids research* **40**: 1050-1064.

Giannattasio M, Branzei D. 2017. S-phase checkpoint regulations that preserve replication and chromosome integrity upon dNTP depletion. *Cellular and molecular life sciences : CMLS* **74**: 2361-2380.

Guo C, Kumagai A, Schlacher K, Shevchenko A, Shevchenko A, Dunphy WG. 2015. Interaction of Chk1 with Treslin negatively regulates the initiation of chromosomal DNA replication. *Molecular cell* **57**: 492-505.

Hamperl S, Bocek MJ, Saldivar JC, Swigut T, Cimprich KA. 2017. Transcription-Replication Conflict Orientation Modulates R-Loop Levels and Activates Distinct DNA Damage Responses. *Cell* **170**: 774-786 e719.

Hamperl S, Cimprich KA. 2014. The contribution of co-transcriptional RNA:DNA hybrid structures to DNA damage and genome instability. *DNA repair* **19**: 84-94.

Holm C, Stearns T, Botstein D. 1989. DNA topoisomerase II must act at mitosis to prevent nondisjunction and chromosome breakage. *Molecular and cellular biology* **9**: 159-168.

Holstein EM, Lawless C, Banks P, Lydall D. 2018. Genome-Wide Quantitative Fitness Analysis (QFA) of Yeast Cultures. *Methods in molecular biology* **1672**: 575-597.

Josse R, Martin SE, Guha R, Ormanoglu P, Pfister TD, Reaper PM, Barnes CS, Jones J, Charlton P, Pollard JR et al. 2014. ATR inhibitors VE-821 and VX-970 sensitize cancer cells to topoisomerase i inhibitors by disabling DNA replication initiation and fork elongation responses. *Cancer research* **74**: 6968-6979.

Kolinjivadi AM, Sannino V, de Antoni A, Techer H, Baldi G, Costanzo V. 2017. Moonlighting at replication forks - a new life for homologous recombination proteins BRCA1, BRCA2 and RAD51. *FEBS letters* **591**: 1083-1100.

Kotsantis P, Petermann E, Boulton SJ. 2018. Mechanisms of Oncogene-Induced Replication Stress: Jigsaw Falling into Place. *Cancer discovery* **8**: 537-555.

Lisby M, Barlow JH, Burgess RC, Rothstein R. 2004. Choreography of the DNA damage response: spatiotemporal relationships among checkpoint and repair proteins. *Cell* **118**: 699-713.

Lisby M, Rothstein R, Mortensen UH. 2001. Rad52 forms DNA repair and recombination centers during S phase. *Proceedings of the National Academy of Sciences of the United States of America* **98**: 8276-8282.

Lopez-Mosqueda J, Maas NL, Jonsson ZO, Defazio-Eli LG, Wohlschlegel J, Toczyski DP. 2010. Damage-induced phosphorylation of Sld3 is important to block late origin firing. *Nature* **467**: 479-483.

728 Malacaria E, Pugliese GM, Honda M, Marabitti V, Aiello FA, Spies M, Franchitto A,
729 Pichierri P. 2019. Rad52 prevents excessive replication fork reversal and
730 protects from nascent strand degradation. *Nature communications* **10**: 1412.

731 Mantiero D, Mackenzie A, Donaldson A, Zegerman P. 2011. Limiting replication
732 initiation factors execute the temporal programme of origin firing in budding
733 yeast. *The EMBO journal* **30**: 4805-4814.

734 McIntosh D, Blow JJ. 2012. Dormant origins, the licensing checkpoint, and the
735 response to replicative stresses. *Cold Spring Harbor perspectives in biology*
736 **4**.

737 Morrison AJ, Shen X. 2009. Chromatin remodelling beyond transcription: the INO80
738 and SWR1 complexes. *Nature reviews Molecular cell biology* **10**: 373-384.

739 Muller CA, Hawkins M, Retkute R, Malla S, Wilson R, Blythe MJ, Nakato R, Komata
740 M, Shirahige K, de Moura AP et al. 2014. The dynamics of genome
741 replication using deep sequencing. *Nucleic acids research* **42**: e3.

742 Neelsen KJ, Lopes M. 2015. Replication fork reversal in eukaryotes: from dead end
743 to dynamic response. *Nature reviews Molecular cell biology* **16**: 207-220.

744 Nitiss JL, Nitiss KC, Rose A, Waltman JL. 2001. Overexpression of type I
745 topoisomerases sensitizes yeast cells to DNA damage. *The Journal of*
746 *biological chemistry* **276**: 26708-26714.

747 Painter RB. 1977. Inhibition of initiation of HeLa cell replicons by methyl
748 methanesulfonate. *Mutation research* **42**: 299-303.

749 Painter RB, Young BR. 1980. Radiosensitivity in ataxia-telangiectasia: a new
750 explanation. *Proceedings of the National Academy of Sciences of the United*
751 *States of America* **77**: 7315-7317.

752 Pardo B, Crabbe L, Pasero P. 2017. Signaling pathways of replication stress in
753 yeast. *FEMS yeast research* **17**.

754 Paulovich AG, Hartwell LH. 1995. A checkpoint regulates the rate of progression
755 through S phase in S. cerevisiae in response to DNA damage. *Cell* **82**: 841-
756 847.

757 Paulovich AG, Toczyski DP, Hartwell LH. 1997. When checkpoints fail. *Cell* **88**: 315-
758 321.

759 Peter BJ, Ullsperger C, Hiasa H, Marians KJ, Cozzarelli NR. 1998. The structure of
760 supercoiled intermediates in DNA replication. *Cell* **94**: 819-827.

761 Poli J, Tsaponina O, Crabbe L, Keszthelyi A, Pantesco V, Chabes A, Lengronne A,
762 Pasero P. 2012. dNTP pools determine fork progression and origin usage
763 under replication stress. *The EMBO journal* **31**: 883-894.

764 Postow L, Ullsperger C, Keller RW, Bustamante C, Vologodskii AV, Cozzarelli NR.
765 2001. Positive torsional strain causes the formation of a four-way junction at
766 replication forks. *The Journal of biological chemistry* **276**: 2790-2796.

767 Pu S, Wong J, Turner B, Cho E, Wodak SJ. 2009. Up-to-date catalogues of yeast
768 protein complexes. *Nucleic acids research* **37**: 825-831.

769 Regairaz M, Zhang YW, Fu H, Agama KK, Tata N, Agrawal S, Aladjem MI, Pommier
770 Y. 2011. Mus81-mediated DNA cleavage resolves replication forks stalled by
771 topoisomerase I-DNA complexes. *The Journal of cell biology* **195**: 739-749.

772 Rhind N, Gilbert DM. 2013. DNA replication timing. *Cold Spring Harbor perspectives*
773 *in biology* **5**: a010132.

774 Schalbetter SA, Mansoubi S, Chambers AL, Downs JA, Baxter J. 2015. Fork rotation
775 and DNA precatenation are restricted during DNA replication to prevent

776 chromosomal instability. *Proceedings of the National Academy of Sciences of*
777 *the United States of America* **112**: E4565-4570.

778 Sen N, Leonard J, Torres R, Garcia-Luis J, Palou-Marin G, Aragon L. 2016. Physical
779 Proximity of Sister Chromatids Promotes Top2-Dependent Intertwining.
780 *Molecular cell* **64**: 134-147.

781 Siow CC, Nieduszynska SR, Muller CA, Nieduszynski CA. 2012. OriDB, the DNA
782 replication origin database updated and extended. *Nucleic acids research* **40**:
783 D682-686.

784 Srivatsan A, Li BZ, Szakal B, Branzei D, Putnam CD, Kolodner RD. 2018. The Swr1
785 chromatin-remodeling complex prevents genome instability induced by
786 replication fork progression defects. *Nature communications* **9**: 3680.

787 Szilard RK, Jacques PE, Laramee L, Cheng B, Galicia S, Bataille AR, Yeung M,
788 Mendez M, Bergeron M, Robert F et al. 2010. Systematic identification of
789 fragile sites via genome-wide location analysis of gamma-H2AX. *Nature*
790 *structural & molecular biology* **17**: 299-305.

791 Tanaka S, Nakato R, Katou Y, Shirahige K, Araki H. 2011. Origin association of Sld3,
792 Sld7, and Cdc45 proteins is a key step for determination of origin-firing timing.
793 *Current biology : CB* **21**: 2055-2063.

794 Tercero JA, Longhese MP, Diffley JF. 2003. A central role for DNA replication forks in
795 checkpoint activation and response. *Molecular cell* **11**: 1323-1336.

796 Thomas A, Redon CE, Sciuto L, Padiernos E, Ji J, Lee MJ, Yuno A, Lee S, Zhang Y,
797 Tran L et al. 2018. Phase I Study of ATR Inhibitor M6620 in Combination With
798 Topotecan in Patients With Advanced Solid Tumors. *Journal of clinical*
799 *oncology : official journal of the American Society of Clinical Oncology* **36**:
800 1594-1602.

801 Tong AH, Boone C. 2006. Synthetic genetic array analysis in Saccharomyces
802 cerevisiae. *Methods in molecular biology* **313**: 171-192.

803 Tuduri S, Crabbe L, Conti C, Tourriere H, Holtgreve-Grez H, Jauch A, Pantesco V,
804 De Vos J, Thomas A, Theillet C et al. 2009. Topoisomerase I suppresses
805 genomic instability by preventing interference between replication and
806 transcription. *Nature cell biology* **11**: 1315-1324.

807 Zegerman P, Diffley JF. 2010. Checkpoint-dependent inhibition of DNA replication
808 initiation by Sld3 and Dbf4 phosphorylation. *Nature* **467**: 474-478.

809 Zhong Y, Nellimoottil T, Peace JM, Knott SR, Villwock SK, Yee JM, Jancuska JM,
810 Rege S, Tecklenburg M, Sclafani RA et al. 2013. The level of origin firing
811 inversely affects the rate of replication fork progression. *The Journal of cell*
812 *biology* **201**: 373-383.

813

Figure 1. Morafraile et al. 328682

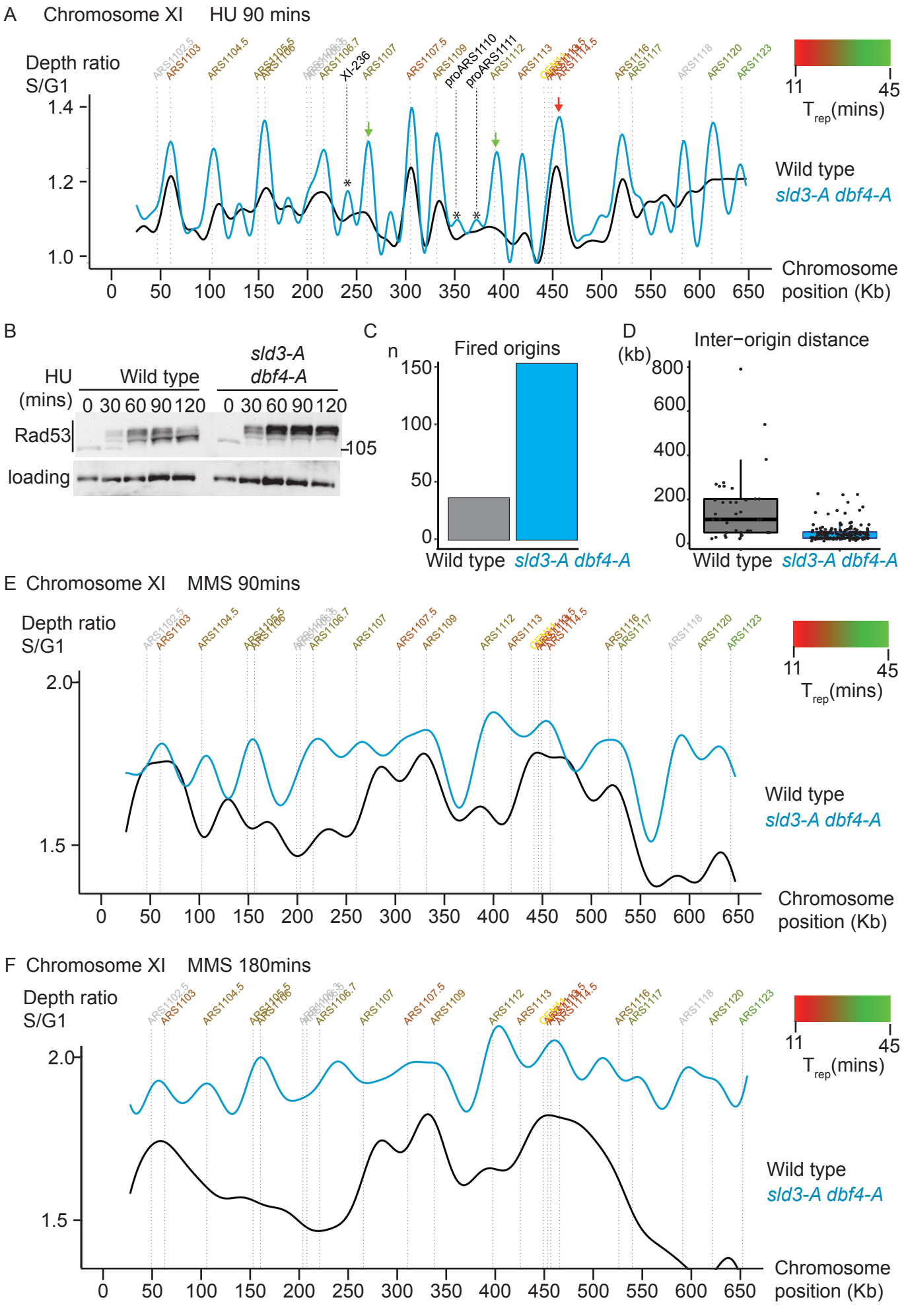

Figure 1. The replication checkpoint inhibits origin firing genome-wide.

A. Replication profile of the indicated strains after release from alpha factor into 200mM HU for 90 minutes. Copy number (y-axis) was derived by normalising the sequencing reads at 90 minutes to the reads at 0 minutes (G1). Annotated origins (top) are coloured according to their average time of replication in an unperturbed S-phase (T_{rep}) from early (red) to late (green). Only chromosome XI is shown for simplicity. Unconfirmed origins also fire in the *sld3-A dbf4-A* strain, examples of which are indicated by the *. The telomeres are excluded due to mappability issues.

B. Rad53 western blot from the indicated strains released from G1 phase arrest with alpha factor (0 mins) into 200mM HU for the indicated time points.

C. Graph of number of origins from A that fired in at least 20% of cells.

D. Box plot of each origin from C plotted according to the distance to its nearest neighbouring fired origin.

E and **F**. As A, except the strains were released from G1 phase into 0.02% MMS for 90 minutes (E) and 180 minutes (F).

Figure 2. Morafraile et al. 328682

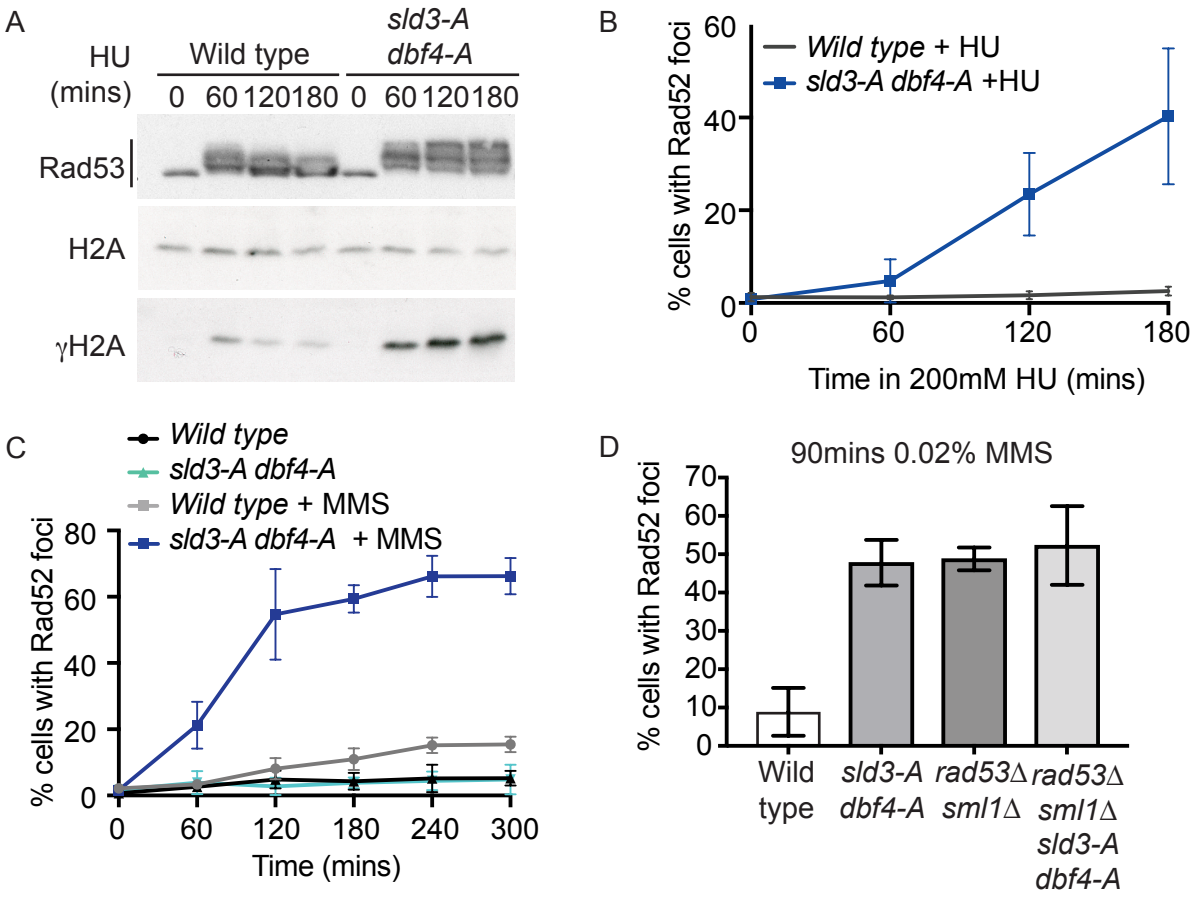

Figure 2. Checkpoint inhibition of origin firing prevents the accumulation of DNA damage markers.
A. Western blots from the indicated strains released from G1 phase arrest with alpha factor (0 mins) into 200mM HU for the indicated time points.
B. Quantification of Rad52-GFP foci in the indicated strains released from G1 phase arrest with alpha factor (0 mins) into 200mM HU for the indicated time points. Error bars are SD, n=7.
C. As B, except strains were released from G1 phase (0 mins) into either 0.02% MMS or into medium in the absence of drug for the indicated time points. Error bars are SD, n=5.
D. Quantification of Rad52-GFP foci in the indicated strains released from G1 phase arrest with alpha factor (0 mins) into 0.02% MMS for 90 minutes. Error bars are SD, n=3.

Figure 3. Morafraile et al. 328682

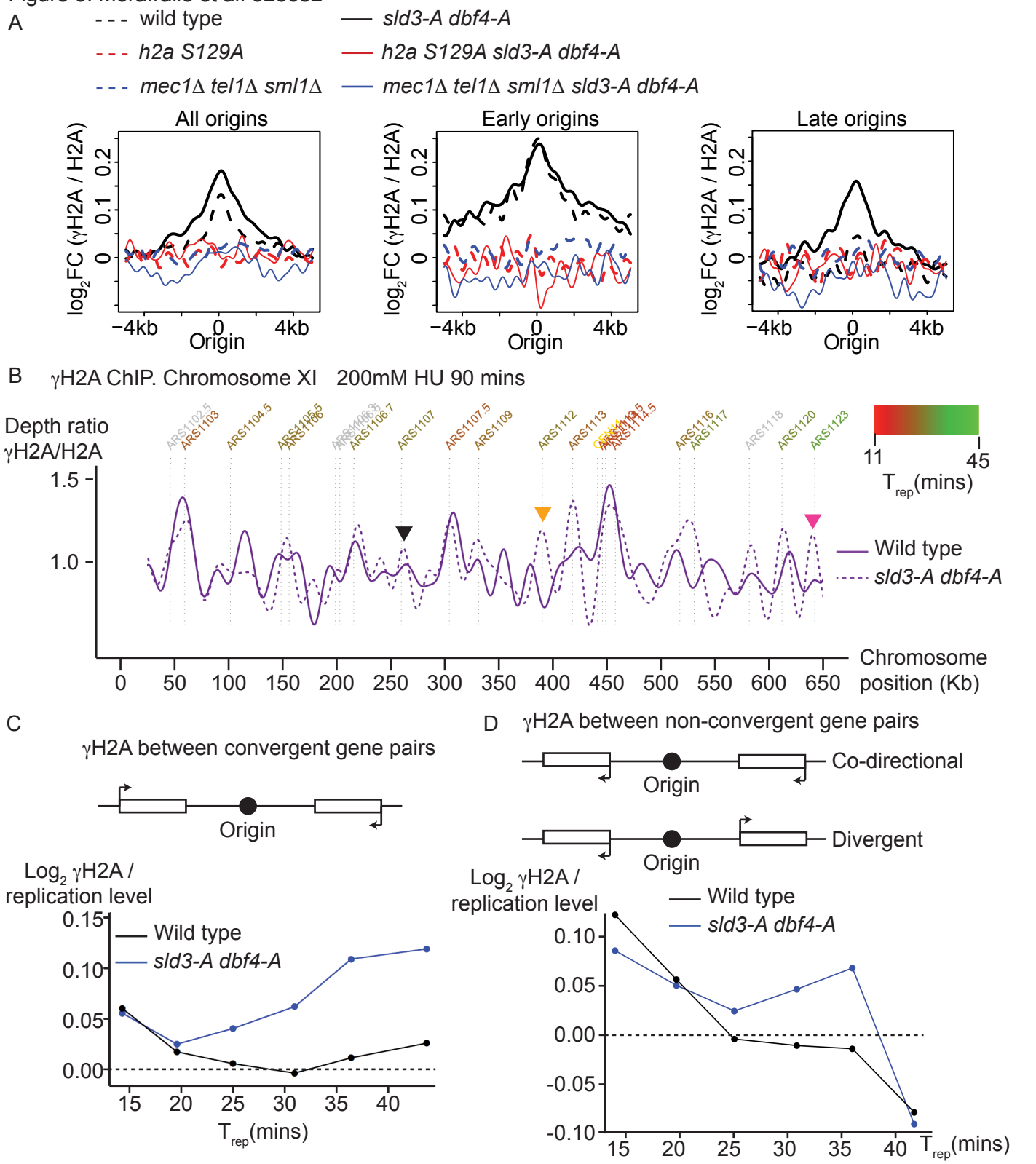

Figure 3. Checkpoint inhibition of origin firing prevents DNA damage globally, but in particular at convergently transcribed gene pairs.

A. Graphs of γH2A ChIP from the indicated strains released from G1 phase arrest into 200mM HU for 90 minutes. The graphs are the average γH2A ChIP signal centred on all origins (left), or origins split into early firing (Trep < 27.5mins, middle) or late firing (Trep > 27.5mins, right). Data is normalised to the ChIP signal of unmodified H2A.

B. Chromosomal view of data from A, only chromosome XI is shown for simplicity. Orange and black arrows indicate origins that fire efficiently in the sld3-A dbf4-A strain, while the pink arrow indicates an origin that does not fire efficiently in the sld3-A dbf4-A strain.

C, D. Schematic diagram of origins between convergently transcribed gene pairs (C, Top), or between co-directional/divergent gene pairs (D, Top). Bottom: γH2A ChIP signal from A was normalised to the amount of replication at that locus. This data was binned according to average time of replication in a normal S-phase (Trep) and separated into those origins that are between convergently transcribed gene pairs (C) or non-convergent gene pairs (D).

Figure 4. Morafraile et al. 328682

A

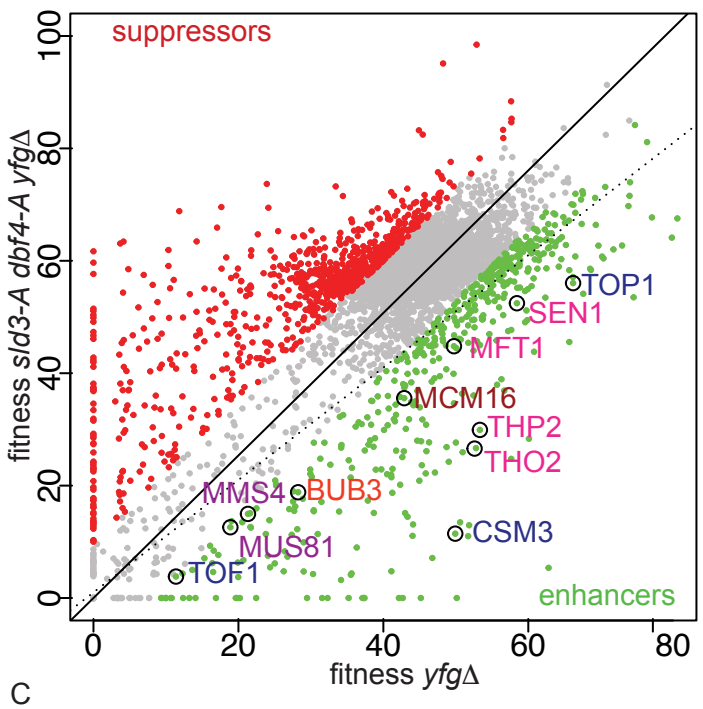

B Complexes from the enhancers in HU

Complex	P-value	Identified subunits
Bub1p/Bub3p complex	0	BUB1 BUB3
DNA polymerase delta	0	POL32 POL3
Elongator complex	0	ELP2 ELP6 ELP3 IKI3 ELP4
Holliday junction resolvase	0	MMS4 MUS81
Rad17p/Ddc1p/Mec3p	0	DDC1 RAD17
THO complex	0	THP2 MFT1 THO2
Tof1p/Mrc1p/Csm3p	0	CSM3 MRC1 TOF1
Swr1p complex	0.009	ARP6 VPS71 SWC3 VPS72 SWC5 SWR1
Mitochondrial sorting and assembly machinery	0.012	SAM37 MDM10 SAM35
DNA replication factor C (Ctf18p/Ctf8p/dcc1p)	0.029	CTF18 CTF8 DCC1 RFC4
Retromer complex	0.049	VPS29 VPS35 PEP8

C

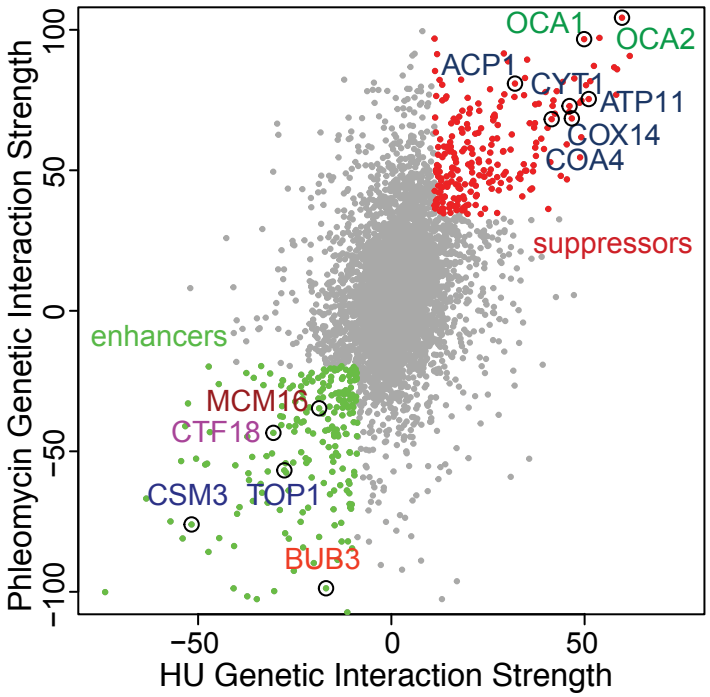

D

Complexes as enhancers in HU and phleomycin

Complex	P-value	Identified subunits
Bub1p/Bub3p complex	0	BUB1 BUB3
Elongator complex	0	ELP2 ELP6 ELP3 IKI3 ELP4
Chz1p/Htz1p/Htb1p	0.02	HTZ1 HTB1
Ctf3p complex	0.02	MCM16 MCM22
Tof1p/Mrc1p/Csm3p	0.02	CSM3 MRC1
Swr1p complex	0.03	ARP6 VPS71 SWC3 SWR1
DNA replication factor C (Ctf18p/Ctf8p/dcc1p)	0.04	CTF18 CTF8 DCC1

Figure 4. Genetic screens identify pathways that are important in the absence of checkpoint-inhibition of origin firing.

A. Scatter plot of the fitness of the yeast genome knock out collection grown in 100mM HU with (y-axis) or without (x-axis) the sld3-A dbf4-A alleles. Each dot corresponds to a different gene deletion. The top 25% of gene deletions (yfg = your favourite gene) that significantly enhance (green) or suppress (red) the fitness of sld3-A dbf4-A are indicated. The line of hypothetical equal fitness (dotted line) and the line of equal growth derived from a population model of the actual fitness of all the strains (solid line) are indicated. Several examples of the enhancer hits are highlighted and colour coded according to complex-/function.

B. Analysis of the enriched protein complexes of the enhancers in A.

C. Genetic interaction strength (GIS) comparison between the screen in A and an equivalent screen performed in 0.5µg/ml phleomycin. Enhancers and suppressors are highlighted as in A. Several examples of the enhancer/suppressor hits are highlighted and colour coded according to complex/function. The suppressors in blue are involved in mitochondrial function.

D. Analysis of the enriched protein complexes of the enhancers in C.

Figure 5. Morafraile et al. 328682

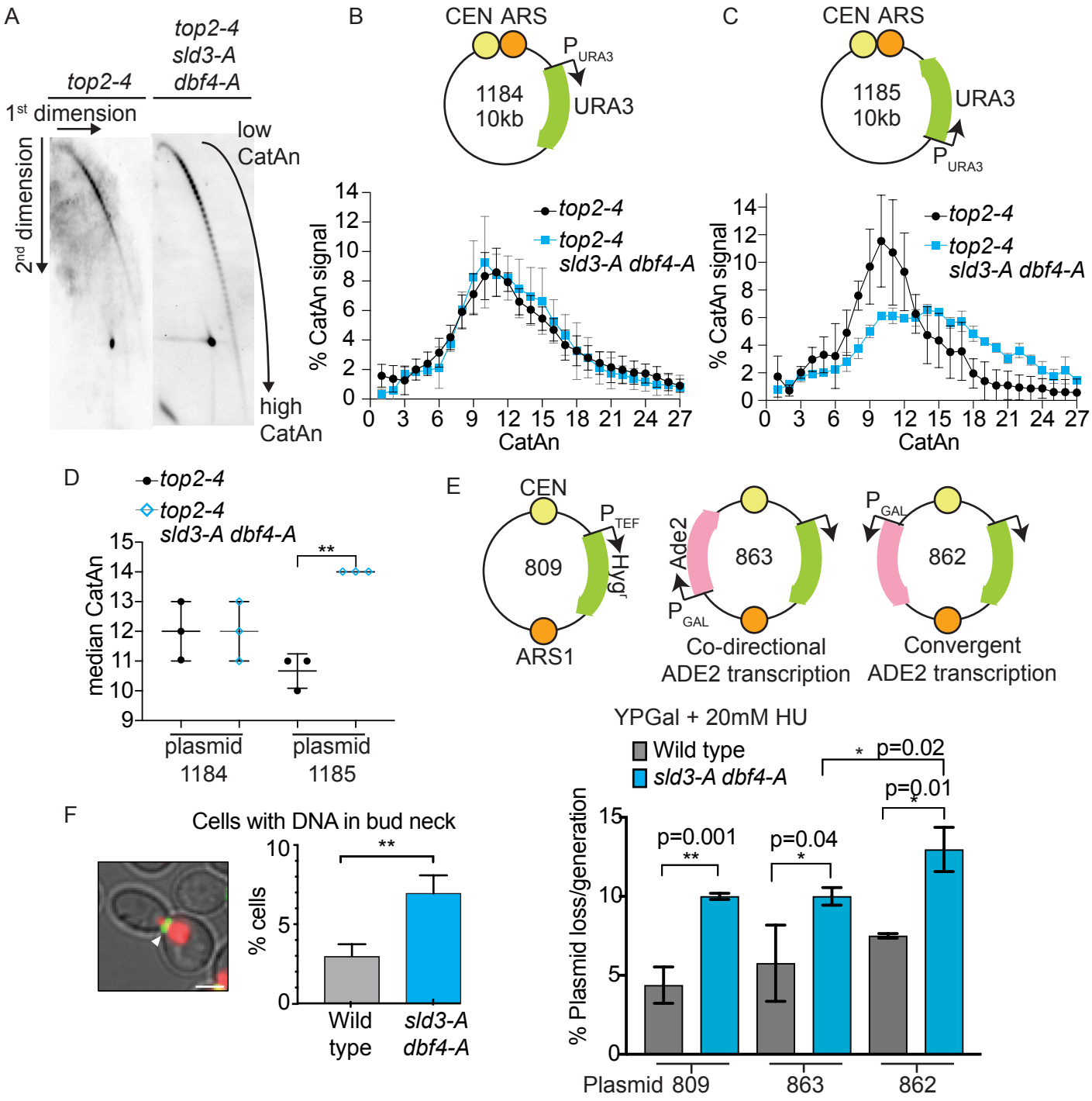

Figure 5. Checkpoint inhibition of origin firing prevents excess catenation and chromosome loss.
A. Southern blots of 2D gels from yeast containing the plasmid 1185 (see C). The indicated yeast strains were arrested in alpha factor at 25oC, then switched to the non-permissive temperature (37oC) for top2-4 and released into 0.033% MMS for 90 minutes. After nicking of DNA to remove supercoiling, the catenated forms (CatA) of the replicated plasmid can be discriminated.
B, C. Top, schematic diagram of plasmids with co-directional (1184) or convergent (1185) URA3 transcription relative to the direction of replication. Bottom, plot of the distribution of catenated isoforms of the plasmids 1184 (B) and 1185 (C) from the indicated strains. Error bars are SD, n=3.
D. Graph of the median CatAn from B and C. Error bars are SD, n=3.
E. Plasmid loss assay of the plasmids shown schematically above. Strains were grown overnight in YP galactose + 20mM HU. Error bars are SD from, n=3. P values are from paired t-tests.
F. Quantification of DNA in the bud neck after cytokinetic ring contraction. Error bars are SD from n=3. Image of yeast (left) containing Htb2-mcherry (red) and myo1-GFP (green). Scale bar is 3μm. A contracted myosin ring was considered to be < 2μm (white arrow).

Figure 6. Morafraile et al. 328682

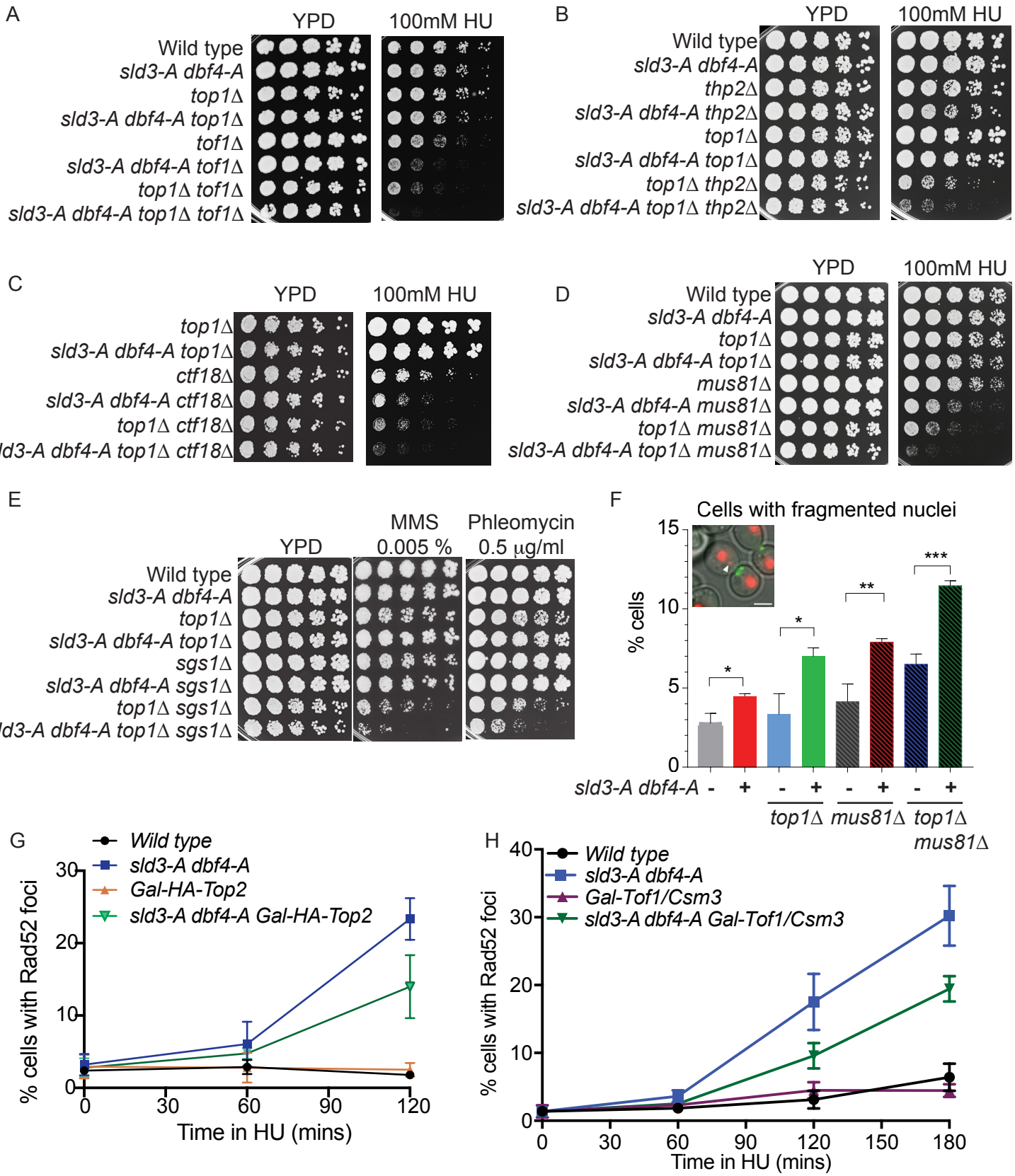

Figure 6. Topological defects explains the genetic interactions and DNA damage in the sld3-A dbf4-A strain.
A-E. 5 fold dilution growth assays of the indicated strains.
F. Quantification of nuclear fragmentation after nuclear separation in the indicated strains. Image of yeast containing Htb2-mcherry (red) and myo1-GFP (green) is shown. Fragmentation was considered only for Htb2 signal that was >0.1μm from the rest of the nucleus (white arrow). Error bars are SD from n=3.
G, H. Quantification of Rad52-GFP foci in the indicated strains released from G1 phase (0 mins) into 200mM HU in YP galactose medium. Error bars are SD, n=3.

Figure 7. Morafraile et al. 328682

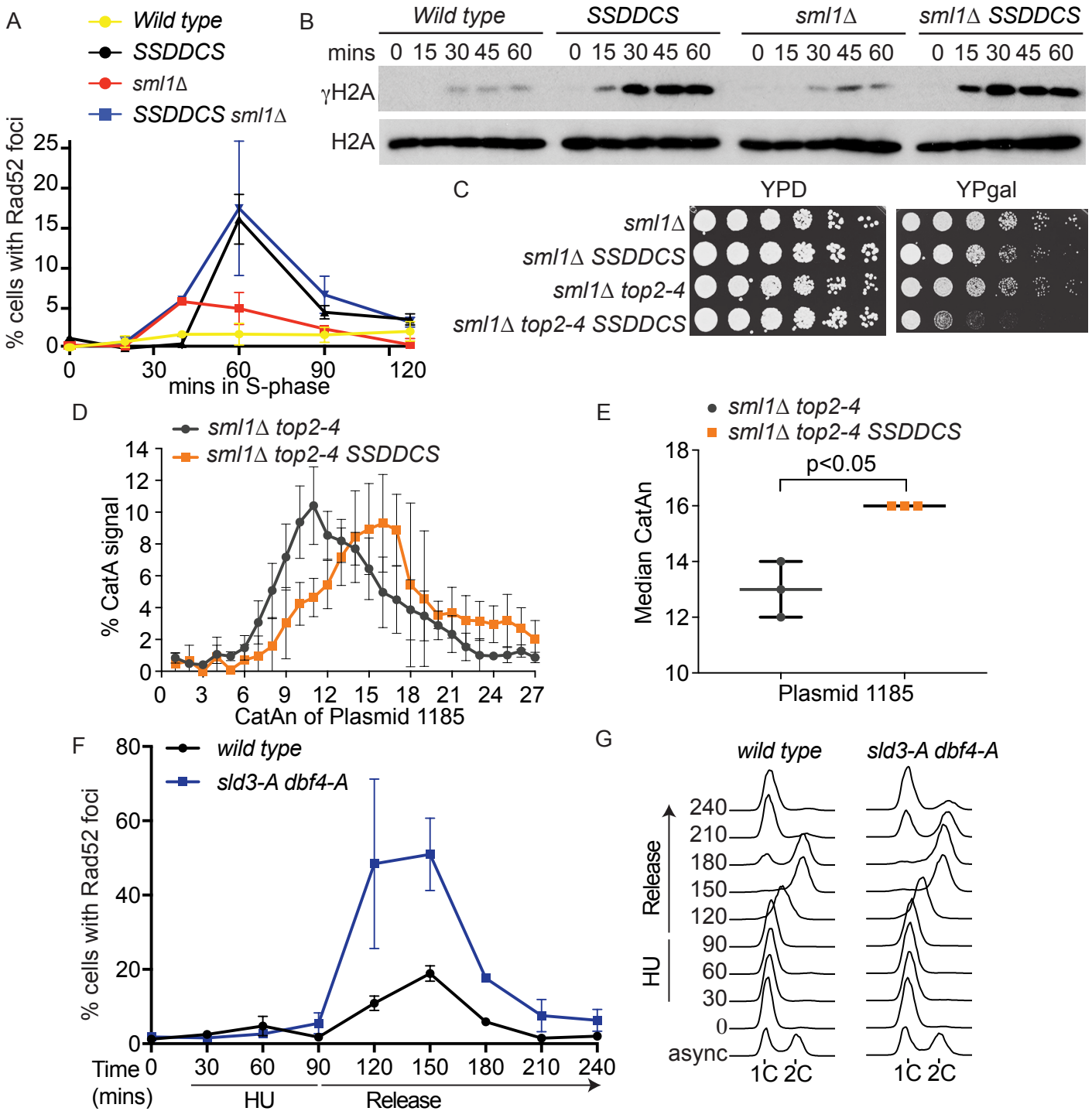

H

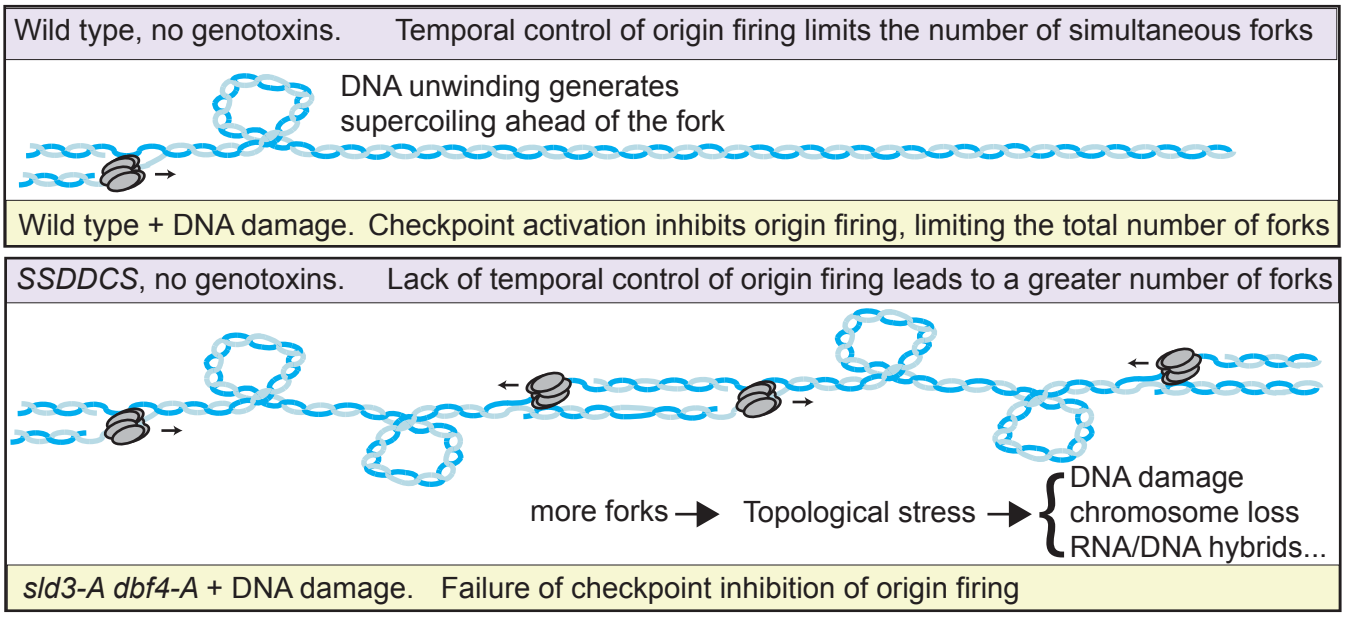

Figure 7. High rates of replication initiation in a normal S-phase causes similar phenotypes to failure of checkpoint inhibition of origin firing

A. Quantification of Rad52-GFP foci in the indicated strains released from G1 phase arrest (0 mins) into YP galactose medium. The SSDDCS strain expresses limiting replication factors from galactose inducible promoters. Error bars are SD, n=3.

B. Western blots of the indicated strains released from G1 phase arrest with alpha factor (0 mins) into YP galactose medium.

C. 5 fold dilution growth assays of the indicated strains in the presence (YPgal) or absence (YPD) of expression of SSDDCS.

D. Plot of the distribution of catenated isoforms of the plasmid 1185 as in Figure 5C. Error bars are SD, n=3.

E. Graph of the median CatAn from D. Error bars are SD, n=3.

F-G. Quantification of Rad52-GFP foci (F) and Flow cytometry (G) of strains released from G1 phase arrest with alpha factor (0 mins) into 200mM HU for 90 mins and then washed into HU-free media (release) for a further 150 minutes. For F, error bars are SD, n=3.

H. Model for the role of origin firing control in preventing topological stress. Wild type cells (top) limit simultaneous fork number in a normal S-phase (purple) through a temporal order of origin firing and after DNA damage (yellow) through the checkpoint inhibition of origin firing. In the absence of the checkpoint inhibition of origin firing (*sld3-A dbf4-A*, yellow, bottom) or in the *SSDDCS* strain in a normal S-phase (purple, bottom), excess origin firing creates topological problems and increased reliance on pathways to remove supercoils and catenanes. Failure to deal with this stress leads to DNA damage/chromosome loss, possibly through increased RNA/DNA hybrid formation or fork reversal.

Supplemental figure 1. Morafraile et al. 328682

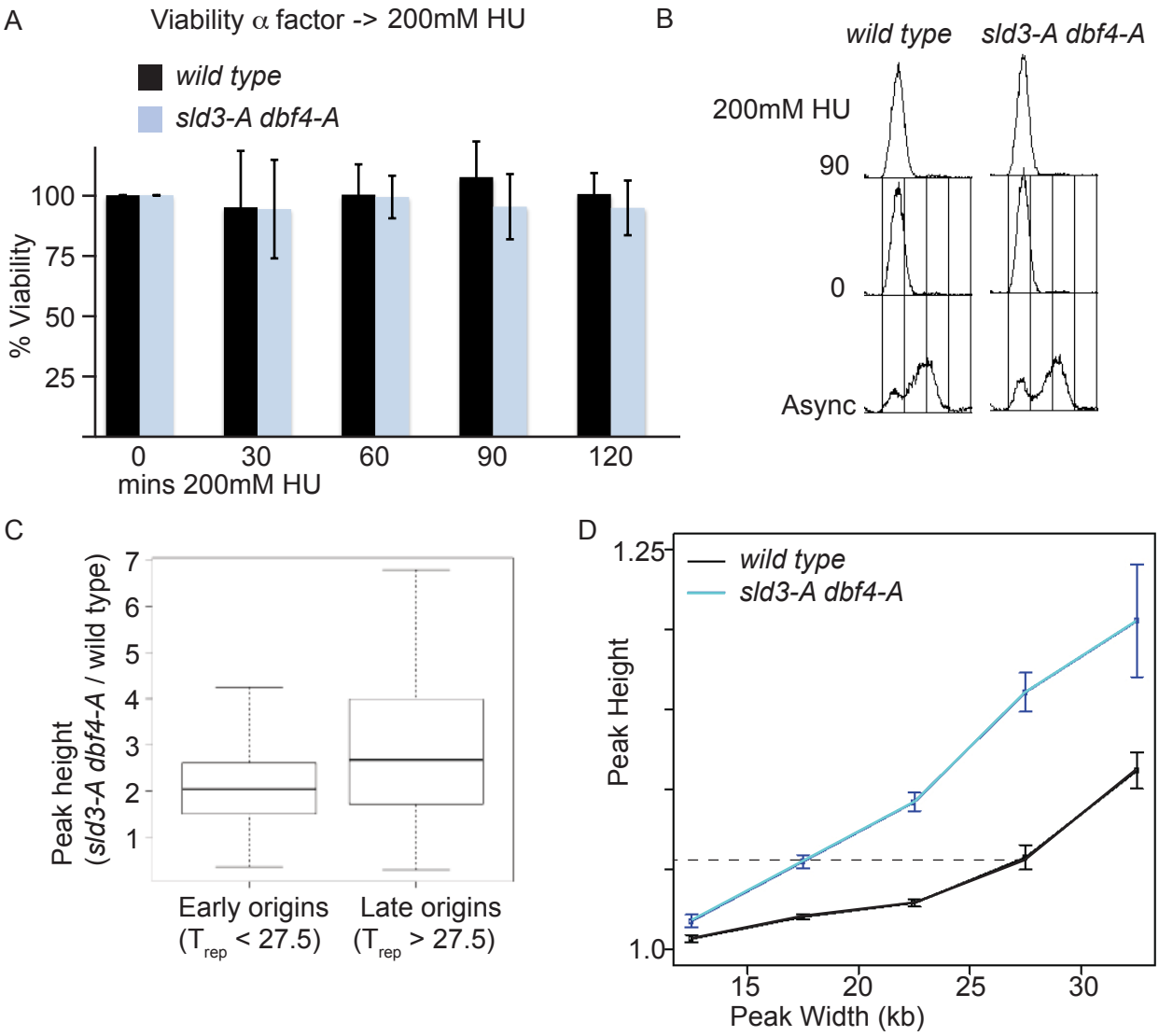

Supplemental figure 2.Morafraile et al. 328682

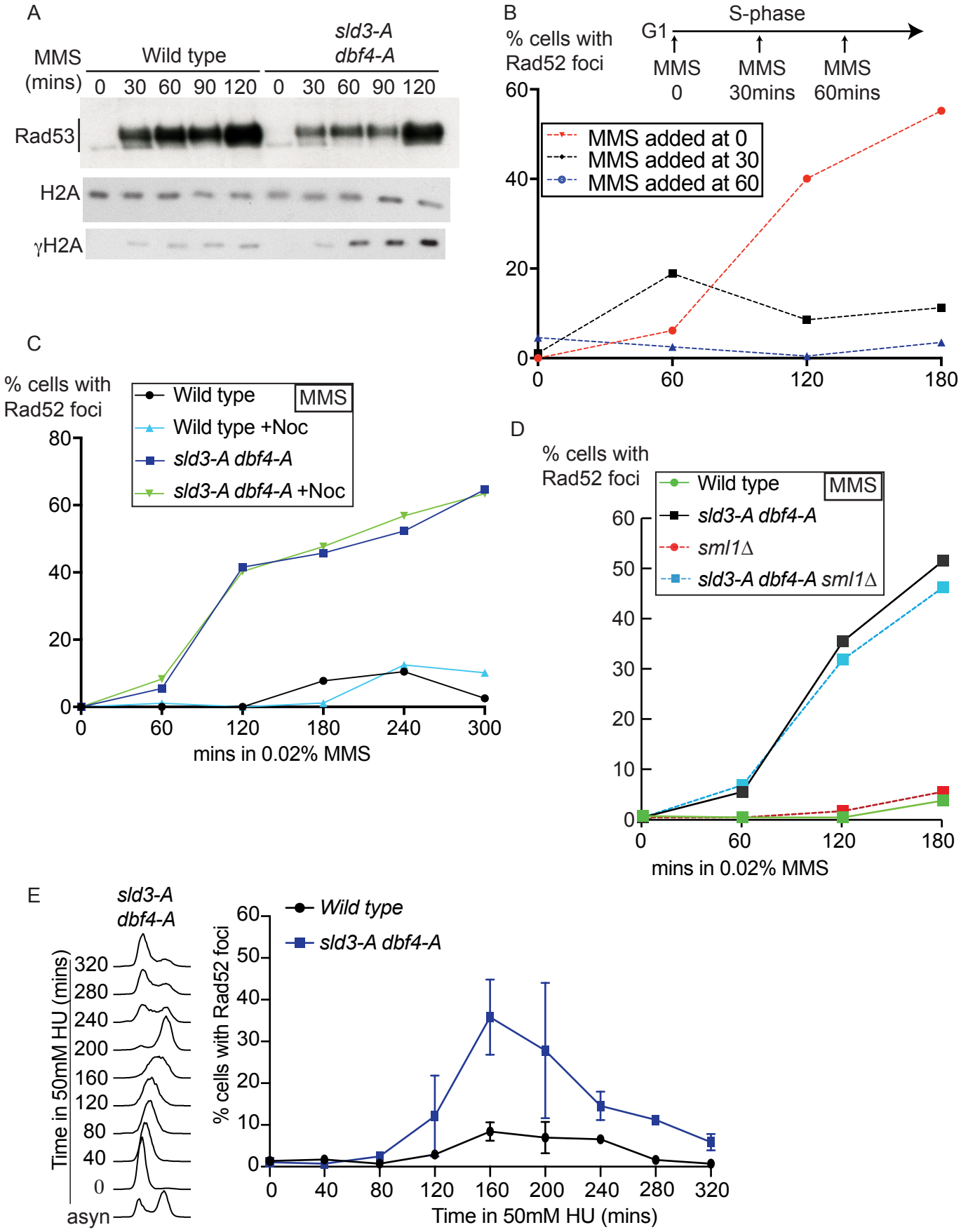

Supplemental Figure 3. Morafraile et al. 328682

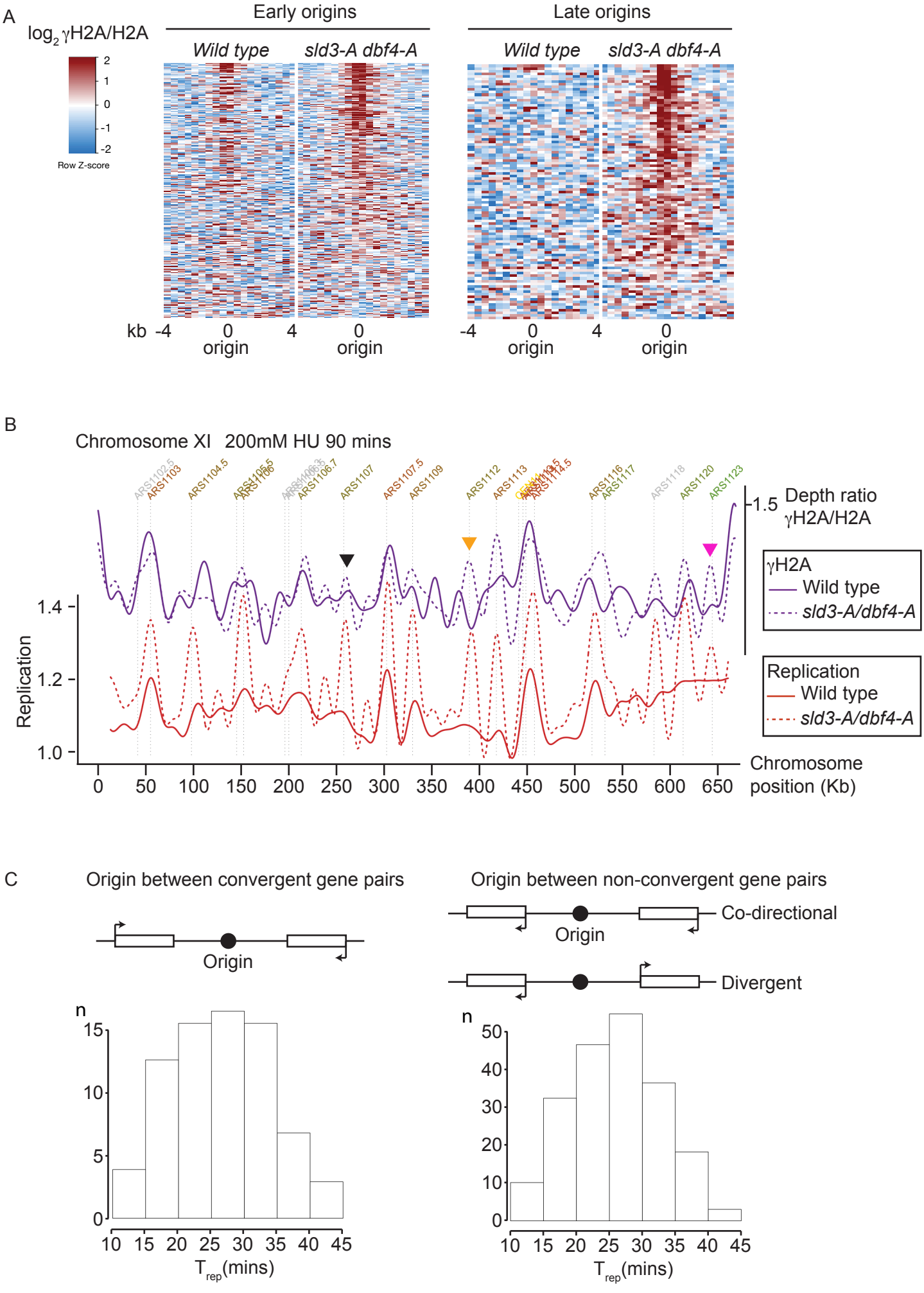

Supplemental Figure 4. Morafraile et al. 328682

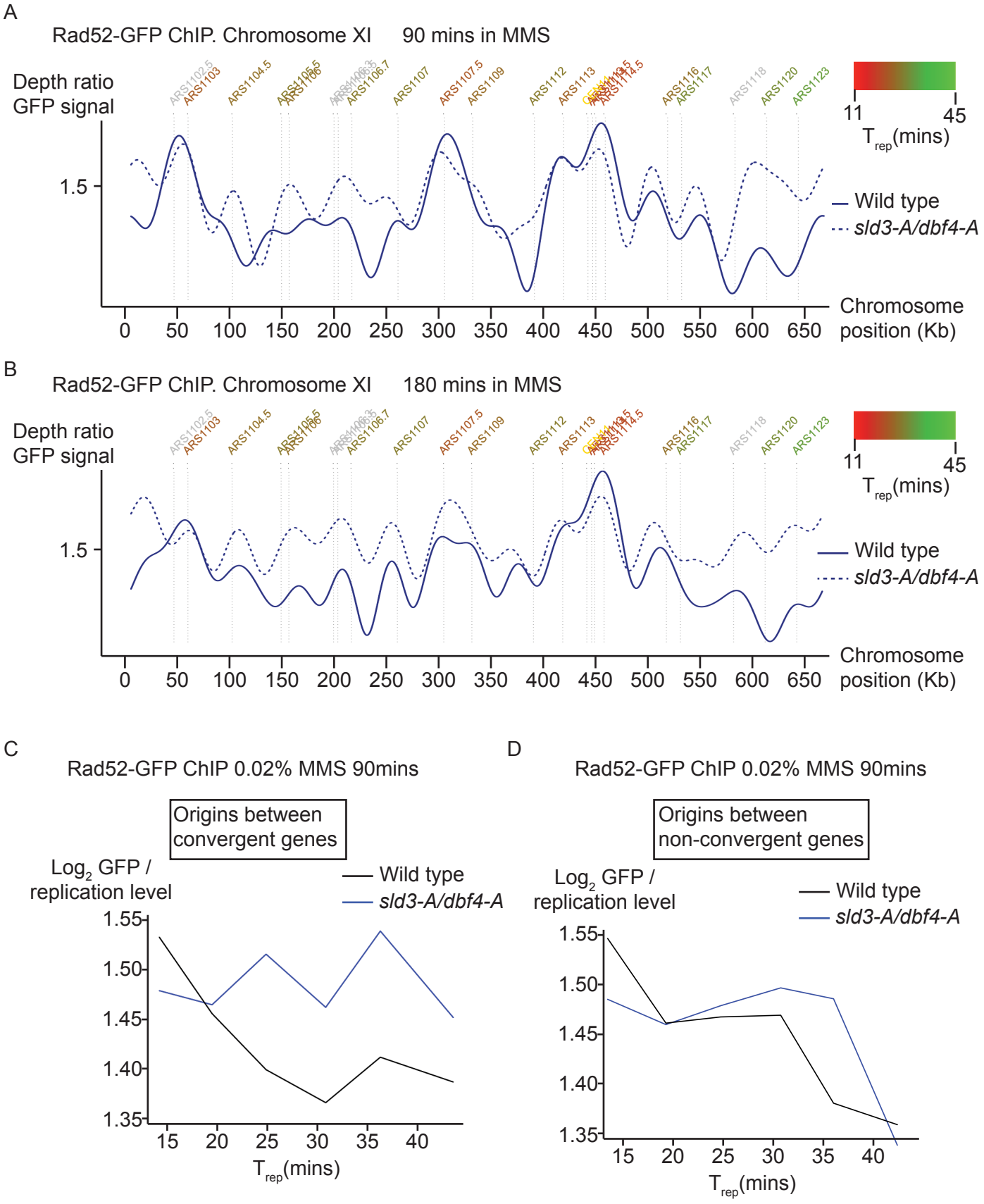

Supplemental Figure 5. Morafraile et al. 328682

A GO analysis of enhancers in HU

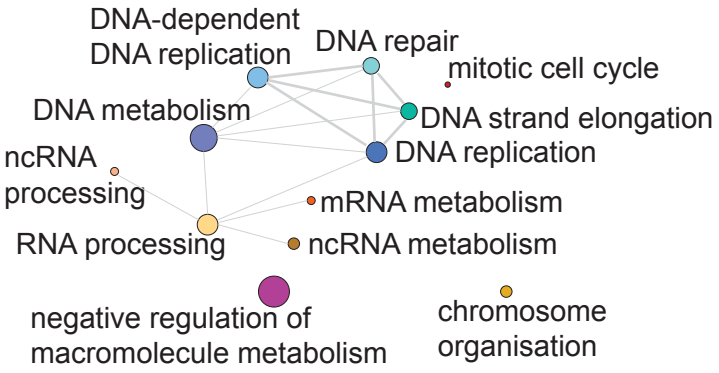

B Overlap between phleomycin and HU screens

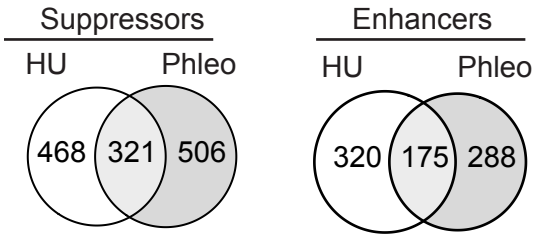

C

Complexes as suppressors in HU and phleomycin

Complex	P-value	Identified subunits
AP-3 adaptor complex	0.00	APS3 , APM3 , APL6
OCA complex	0.01	OCA1 , OCA2
Snf1p/Snf4p/Gal83p complex	0.01	SNF1 , SNF4
prefoldin complex	0.04	PAC10 , GIM5

D

Mutant	Repair pathway	DNA damaging agents			
		MMS	Phleo	4-NQO	CPT
Rad52Δ	HR				
Ku70Δ	NHEJ				
Exo1Δ	Multiple pathways				
Sae2Δ	HR				
Rad50Δ	HR				
Rev3Δ	TLS				
Apn1Δ	BER				
Rad23Δ	NER				
Msh2Δ	MMR				
Rnh201Δ	rNTPs/Rloops				
Rad5-G535R	PRR				

	Synthetic sick > 5-fold growth difference		Suppression 2-5 fold growth difference		No interaction
	Synthetic sick 2-5 fold growth difference		Suppression > 5-fold growth difference		Not analysable due to insufficient growth

Supplemental figure 6. Morafraile et al. 328682

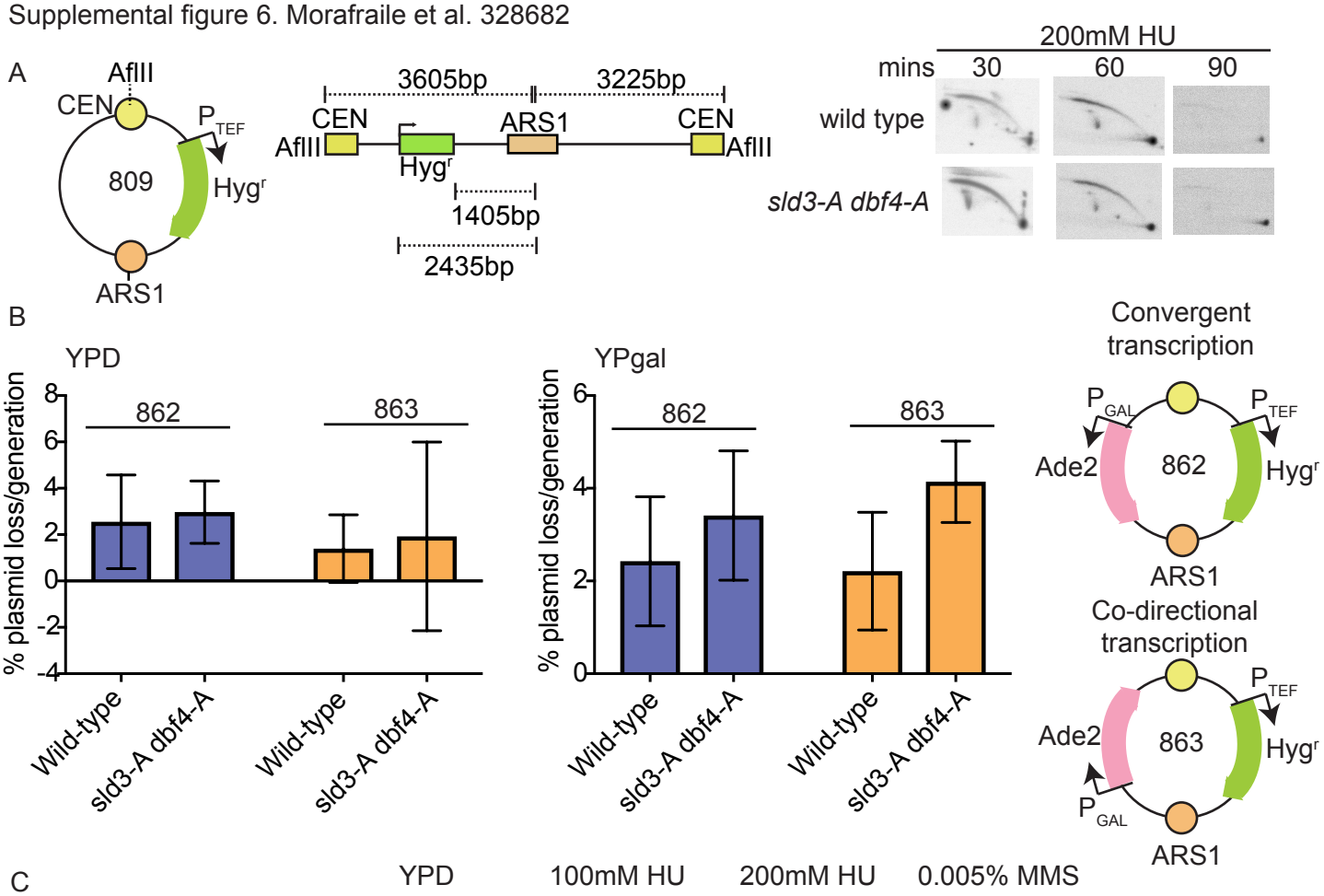

Supplemental Figure 7. Morafraile et al. 328682

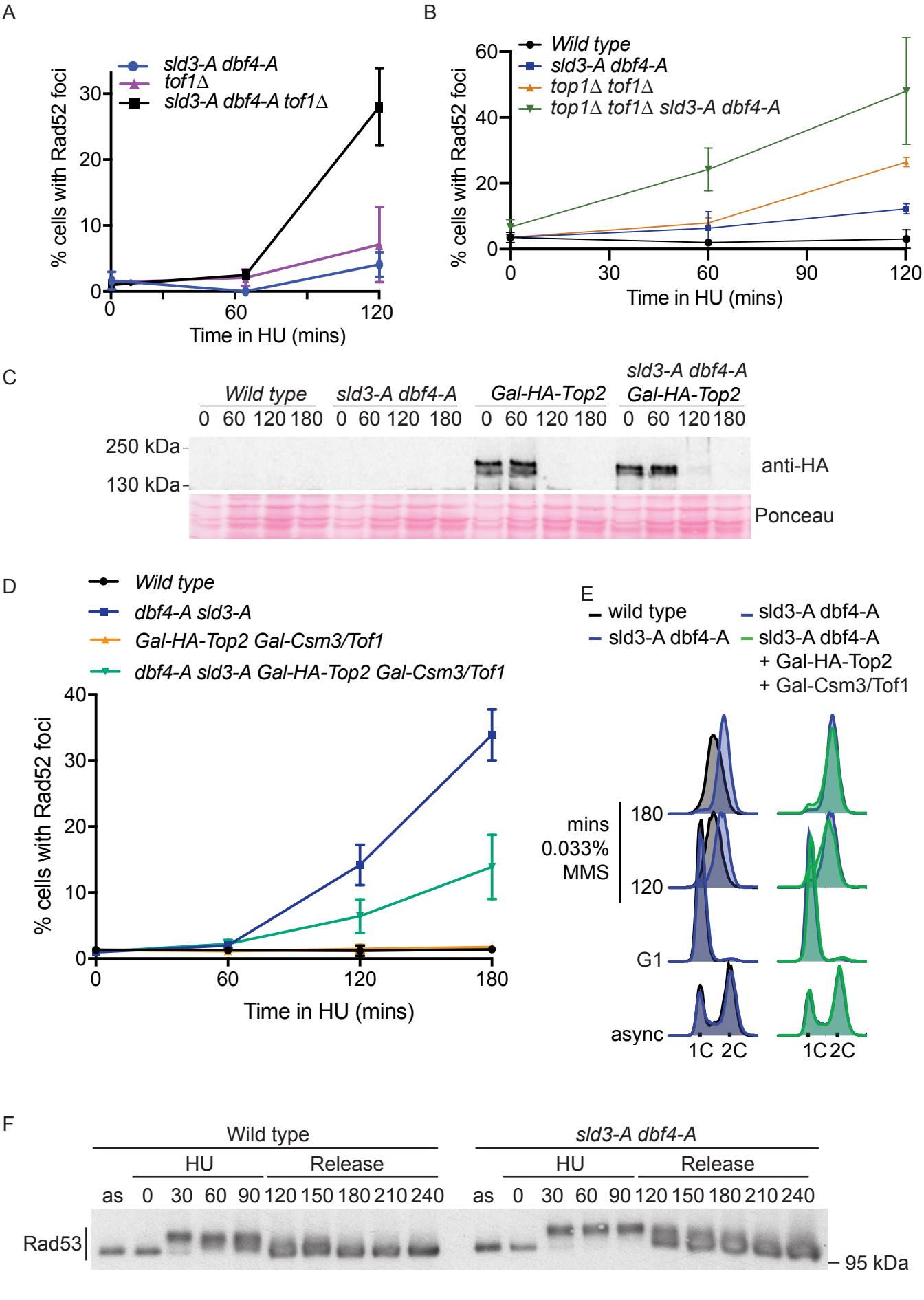

Supplemental Figure Legends

Supplemental Figure 1. *sld3-A dbf4-A* are effective separation of function mutants and prevent the checkpoint inhibition of origin firing globally.

A. Viability analysis of strains arrested in G1 phase arrest with alpha factor (0 mins) and then released into 200mM HU for the indicated times. For each time point 200 cells were plated onto YPD plates in duplicate to count colony growth (viability) after 2 days. The number of colonies at time 0 was set to 100%. Errors bars are SD, n=4. This shows that the *sld3-A dbf4-A* strain has wild type viability in HU, consistent with these alleles having normal replication functions and that other aspects of checkpoint function, such as fork stabilisation are not affected in this strain.

B. Flow cytometry of the experiment in Figure 1A.

C. Box plot of the peak heights of the *sld3-A dbf4-A* strain, divided by the wild type from Figure 1A. Data was binned into those origins that normally fire early or late (less than or more than the median T_{rep} value of 27.5 mins). Horizontal lines are median values, error bars are SD.

D. The peak widths from Figure 1A was binned by kb (x-axis) and was plotted against average peak height for that bin (y-axis). This graph shows that for a given peak height (see dotted line for example) peaks are wider in the wild type strain than in the *sld3-A dbf4-A* strain. Therefore although there are many more forks in the *sld3-A dbf4-A* strain, forks on average move less far in the *sld3-A dbf4-A* strain than in the wild type. Error bars are SD.

E. Flow cytometry of the experiment in Figure 1E/F. The *sld3-A dbf4-A* strain allows for a faster S-phase in the presence of MMS.

Supplemental Figure 2. Failure to inhibit origin firing in HU/MMS results in the accumulation of DNA damage markers.

A. Western blots from the indicated strains released from G1 phase arrest with alpha factor (0 mins) into 0.02% MMS for the indicated time points.

B. Quantification of Rad52-GFP foci in the *sld3-A dbf4-A* strain released from G1 phase arrest with alpha factor (0 mins). 0.02% MMS was either added to the culture immediately after release from G1 (0) or in mid to late S-phase (30 or 60 mins). Rad52-GFP foci accumulate in the *sld3-A dbf4-A* strain when MMS is added before S-phase begins (0).

C. As B. Addition of nocodazole to inhibit anaphase does not suppress the appearance of Rad52 foci in the *sld3-A dbf4-A* strain.

D. As B. Increasing nucleotide pools, through deletion of the RNR inhibitor *SML1*, does not suppress the appearance of Rad52 foci in the *sld3-A dbf4-A* strain.

E. As B, except strains were released into 50mM HU. The flow cytometry of the *sld3-A dbf4-A* strain from this experiment is shown on the left. Error bars are SD, n=3.

Supplemental Figure 3. Checkpoint inhibition of origin firing prevents DNA damage globally, in particular at convergently transcribed genes

A. The γH2A ChIP data from Figure 3A represented as a heatmap, centred on the origin, with 4kb either side. Early origins have a T_{rep} value < 27.5 mins, late origins have a T_{rep} value > 27.5 mins.

B. Overlay of the replication data from Figure 1A (red) with the γH2A ChIP data Figure 3B (purple). This shows sites that are highly replicated in the *sld3-A dbf4-A* strain, but accumulate little γH2A (e.g black arrow) or vice versa (e.g pink arrow).

C. (Top) Schematic diagram of an origin situated between a convergently transcribed pair of genes (left) or a non-convergently transcribed pair of genes (right). Non-convergent transcripts can be either co-directional with respect to each other or divergent. (Below) Histogram of the gene pairs surrounding all origins binned according their median time of replication in a normal S-phase (T_{rep}). Convergent or non-convergent gene pairs show no differences in the T_{rep} of the neighbouring origin.

Supplemental Figure 4. Rad52-GFP ChIP confirms that checkpoint inhibition of origin firing prevents DNA damage globally, in particular at convergently transcribed gene pairs.

A and **B.** Anti-GFP ChIP of Rad52-GFP from the indicated strains, after release from alpha factor into 0.02% MMS for 90 (A) or 180 minutes (B). Only chromosome XI is shown for simplicity.

C and **D**. The GFP ChIP signal at origins from A was binned according to their average time of replication in a normal S-phase (T_{rep}). The data is split between those loci that contain convergent gene pairs (C) or non-convergent gene pairs (D). The y-axis is the GFP signal normalised to the amount of replication at that genomic locus.

Supplemental Figure 5. Genetic screens identify pathways that are important in the absence of checkpoint-inhibition of origin firing.

A. GO analysis of the enhancer hits from the fitness screen in HU with the yeast genome knock out collection from Figure 4A.

B. Venn diagram of the overlap of the statistically significant hits from the HU and Phleomycin whole genome genetic screens.

C. Analysis of the enriched protein complexes from the suppressors in Figure 4C.

D. Targeted genetic analysis of repair pathway mutations in combination with *sld3-A dbf4-A* in yeast strain W303. Data from 5-fold growth dilution assays as in Figure 6A-E are summarised here as a table, colour coded according to whether any genetic interaction was observed between *gene*Δ and the *gene*Δ *sld3-A dbf4-A* triple mutant. All strains apart from *rad5-G535R* are *RAD5*$^{+}$.

Supplemental Figure 6. Plasmid loss is not affected in the *sld3-A dbf4-A* strain in the absence of replication stress and topological defects explains the genetic interactions in the sld3-A dbf4-A strain

A. 2D gel analysis of the plasmid 809 (left) digested with AflII from the indicated strains released from alpha factor into 200mM HU. A scale diagram of the plasmid after linearization with AflII is shown (middle). As expected, episomal plasmids replicate early and therefore fire equally in the wild type and the *sld3-A dbf4-A* strain.

B. Plasmid loss analysis of the indicated plasmids in the absence of genotoxic stress. In the absence of checkpoint activation, a normal temporal programme of origin firing occurs and the wild type and *sld3-A dbf4-A* strains therefore have the same plasmid loss rates. Comparison between YPD and YP + galactose, which induces transcription from the Ade2 gene on the plasmid, shows no effect of transcription specifically on plasmid loss in the *sld3-A dbf4-A* strain in the absence of genotoxic stress. Errors bars are SD, n=3.

E-G. 5 fold dilution growth assays of the indicated strains.

Supplemental Figure 7. Topological defects explains the DNA damage in the sld3-A dbf4-A strain

A and **B**. Quantification of Rad52-GFP foci in the indicated strains released from G1 phase arrest with alpha factor (0 mins) into 200mM HU. Error bars are SD, n=3.

C. Anti-HA western blot of HA-Top2 expressed from the GAL1-10 promoter in cells released from alpha factor (0) into 200mM HU in YPgalactose for the indicated time points. HA-Top2 protein is notably unstable under these conditions.

D. As A/B

E. Overlay of the flow cytometry profile from the indicated strains released from G1 phase into 0.033% MMS. As expected, the wild type strain has a slow S-phase in MMS due to checkpoint inhibition of origin firing, while the *sld3-A dbf4-A* strain completes S-phase progression (left overlay). The *sld3-A dbf4-A* strain that over-expresses HA-Top2 and Csm3/Tof1 also completes S-phase in MMS, indicating that this over-expression does not suppress the excess origin firing caused by the *sld3-A dbf4-A* alleles (right overlay).

F. Rad53 western blot of the experiment in Figure 7F/G. The indicated strains were released from G1 phase arrest with alpha factor (0 mins) into 200mM HU for 90 mins and then washed into HU-free media (release) for a further 150 minutes.